symmetry

MDPI

Review

Dark Photon Searches via Higgs Boson Production at the LHC and Beyond

Sanjoy Biswas [1], Emidio Gabrielli [2,3,4,*] and Barbara Mele [5]

[1] School of Mathematical Sciences, Ramkrishna Mission Vivekananda Educational and Research Institute, P.O. Belur Math, Howrah 711202, India; sanjoy.biswas@rkmvu.ac.in
[2] Dipartimento di Fisica Teorica, Università di Trieste, Strada Costiera 11, I-34151 Trieste, Italy
[3] INFN, Sezione di Trieste, Via Valerio 2, I-34127 Trieste, Italy
[4] NICPB, Rävala 10, 10143 Tallinn, Estonia
[5] INFN, Sezione di Roma, c/o Dipartimento di Fisica, Sapienza Università di Roma, Piazzale Aldo Moro 2, I-00185 Rome, Italy; barbara.mele@roma1.infn.it
* Correspondence: emidio.gabrielli@cern.ch

Abstract: Many scenarios beyond the standard model, aiming to solve long-standing cosmological and particle physics problems, suggest that dark matter might experience long-distance interactions mediated by an *unbroken* dark $U(1)$ gauge symmetry, hence foreseeing the existence of a *massless* dark photon. Contrary to the massive dark photon, a *massless* dark photon can only couple to the standard model sector by means of effective higher dimensional operators. Massless dark photon production at colliders will then in general be suppressed at low energy by a UV energy scale, which is of the order of the masses of portal (messenger) fields connecting the dark and the observable sectors. A violation of this expectation is provided by dark photon production mediated by the Higgs boson, thanks to the non-decoupling Higgs properties. Higgs boson production at colliders, followed by the Higgs decay into a photon and a dark photon, provides then a very promising production mechanism for the dark photon discovery, being insensitive in particular regimes to the UV scale of the new physics. This decay channel gives rise to a peculiar signature characterized by a monochromatic photon with energy half the Higgs mass (in the Higgs rest frame) plus missing energy. We show how such resonant photon-plus-missing-energy signature can *uniquely* be connected to a dark photon production. Higgs boson production and decay into a photon and a dark photon as a source of dark photons is reviewed at the Large Hadron Collider, in light of the present bounds on the corresponding signature by the CMS and ATLAS collaborations. Perspectives for the dark photon production in Higgs-mediated processes at future e^+e^- colliders are also discussed.

Keywords: dark sector; dark photon; Higgs boson; LHC; FCCee

Citation: Biswas, S.; Gabrielli, E.; Mele, B. Dark Photon Searches via Higgs Boson Production at the LHC and Beyond. *Symmetry* **2022**, *14*, 1522. https://doi.org/10.3390/sym14081522

Academic Editor: Theodota Lagouri

Received: 30 May 2022
Accepted: 19 July 2022
Published: 26 July 2022

1. Introduction

The discovery of the Higgs boson in 2012 at the Large Hadron Collider (LHC) by the ATLAS [1] and CMS [2] collaborations has been a milestone for particle physics and the triumph of the Standard Model (SM) of electroweak (EW) and strong interactions [3,4]. The good experimental agreement with the SM Higgs expectations has strengthened our confidence in the Higgs mechanism and in the existence of the Yukawa couplings to fermions, needed for the fermion mass generation in the SM framework [5,6]. Recent results from the LHC data analysis have further consolidated these expectations [7–14]. In particular, the observations of the Higgs boson decay modes into bottom-quark [8–10] and tau-lepton pairs [11,12], as well as the detection of the Higgs boson production in association with top-quark pairs [13,14], are all consistent with the hypothesis of a SM Yukawa coupling strength, thus supporting the existence of the corresponding interactions in nature.

Despite the good SM agreement with data, we are still far from a complete understanding of the Higgs boson physics and of its properties. Regardless of the Higgs boson discovery, a few major intriguing puzzles, highlighted below, are still to be clarified.

- According to the common wisdom, New Physics (NP) at the TeV scale, charged under the SM interactions, is needed to stabilize the electroweak vacuum against potentially large quantum corrections to the Higgs potential, often referred to as the *fine-tuning* problem (see for instance [15–17]). So far, no such NP has been discovered at the LHC, raising doubts about our understanding of *naturalness* [18] in quantum field theory.
- The SM does not contain suitable dark matter candidates. Although dark matter is five times more abundant than ordinary baryonic matter [19–24], its properties are yet unknown.
- An underlying mechanism explaining the origin of the large hierarchy among fundamental fermion masses, or analogously their Yukawa couplings, including the origin of the small neutrino masses and flavor mixing, is missing in the SM.

While the fine-tuning issue might be an ill-defined problem, as recently emphasized in [25], the presence of dark matter in the universe is real experimental evidence for NP [19–24] in case its nature is explained by the presence of new weakly interacting constituents of non-baryonic origin beyond neutrinos, which are missing in the SM spectrum.

Despite its growing evidence, the non-gravitational nature of dark matter remains a mystery, so far eluding all *direct* [20,26–29] and *indirect* (i.e., based on the search for annihilation or decay debris of hypothetical dark matter particles [30,31]) detection. This factual observation has recently opened the way to more speculative approaches about its origin. One intriguing possibility is that dark matter could be linked to the presence of a *dark sector* beyond the SM [32–43]. A dark sector is made of states that are singlets under the SM gauge groups and can also have its own structure and interactions. Indeed, dark matter might even be charged under its own long-range force (that is not experienced by SM particles), mediated for instance by a hidden $U(1)$ gauge symmetry in the dark sector [44]. Speculative approaches in this direction have been motivated in part by potential discrepancies in conventional dark matter scenarios (especially on small scales) but also by the fact that *charged* dark matter could help explain galaxy formation and dynamics [45–48].

The interest for dark sector searches goes beyond the purposes of astrophysics and cosmology, as shown by a number of recent reports on the subject [49–58], covering also searches for long-lived particles [59] and millicharged particles [60–63]. New phenomenological evidence supporting the possible existence of a dark sector are growing. Recently, a new excess in the electronic recoil data was observed in the XENON1T detector that could be explained by the presence of a dark photon [64–69], associated to the quanta of a $U(1)$ long-range force in the dark sector, with mass of the order of 2–3 keV [70,71].

From the side of flavor physics, all quark-flavor and CP-violating experiments over the last 40 years have confirmed the correctness of the SM description via the Higgs Yukawa interactions for fundamental fermions [72,73]. On the other hand, the large fermion-masses (or, analogously, Yukawa-couplings) spectrum, which spans over six orders of magnitude for charged fermions (and even more if neutrinos have only Dirac masses just as quarks and charged leptons) still remains a mystery. The lack of any mechanism in the SM to naturally explain this hierarchy might well suggest the presence of NP behind it. Although the discovery of non-vanishing neutrino masses can hint at a new intermediate scale between the weak and the Planck scale via the seesaw mechanism, the latter also cannot explain the large gap in the charged-fermion sector.

A new paradigm for the flavor genesis [74,75] has been recently proposed suggesting that SM fermion masses, flavor mixing [76], and dark matter constituents might have a common origin in a dark sector. If correct, this paradigm can provide the missing link between some of the long-standing puzzles in particle physics and the existence of dark sectors. The key idea is based on the assumption that the Yukawa couplings are not fundamental couplings, but rather effective ones, radiatively induced by a dark sector. The absence of any tree-level Yukawa operator is guaranteed by some local or global

symmetry which eventually is spontaneously broken by the vacuum expectation value (vev) μ of some scalar field. Contrary to the SM case, for energies above the μ scale, the Yukawa operators cease to exist as local operators. [The mechanism to generate effective Yukawa couplings aiming to explain the hierarchy problem has been previously considered. Known attempts in the literature are mainly based on the Nielsen–Froggatt mechanism [77] or confining different fermions in different branes located in different places in extra dimensions [78]. However, these mechanisms are both affected by the presence of non-renormalizable interactions (in four dimensions), while the approach in [74] is based on a fully renormalizable theory in four dimensions].

To radiatively generate Yukawa couplings at one loop from a dark sector, a set of messengers fields—charged under SM gauge interactions and with same quantum numbers as squarks and sleptons in supersymmetric (SUSY) models—is required to communicate interactions between the dark and SM observable sectors. Massive vector-like dark fermion fields, heavier SM gauge-singlet replicas of the SM fermions, are also needed [74], with their masses playing the role of the chiral symmetry breaking parameters. Thus, dark fermions turn out to be almost a heavy replica of the SM fermions, provided the messenger sector is flavor blind. All dark fermions, as well as messenger fields, are also charged under an unbroken $U(1)_D$ dark-gauge interaction [$U(1)_D$ gauge symmetry was introduced in [74] for dynamical reasons. Indeed, it was shown that a particular non-perturbative dynamic in the $U(1)_D$ sector can generate an exponentially suppressed spectra of dark fermions, as a function of the $U(1)_D$ quantum charges (that are parameters of order $\mathcal{O}(1)$), thus naturally solving the flavor hierarchy problem according to the naturalness criteria of [18]. See [74,79] for more details.], which automatically ensures dark fermions stability. The presence of long-range interacting multi-dark matter constituents comes out as one of the main features of this scenario.

It was also recently shown [80] that the presence of a radiative Yukawa coupling for the top quark in this framework can fully stabilize the Higgs scalar potential, naturally solving the problem of the vacuum instability of the SM Higgs sector [81–87] without a particular tuning of the parameters.

From considerations based on general grounds, the SM fields can couple to the dark sector fields by means of higher dimensional operators, whose associated effective scale Λ is expected to be proportional to the average mass of the corresponding messenger sector. Therefore, the sensitivity to the dark sector searches at low energies E is expected to be suppressed by some powers of E/Λ that depend on the dimension of the operator involved.

A deviation from this rule is provided by the coupling of the dark photon, the quanta associated to the corresponding field of the $U(1)_D$ gauge interaction in the dark sector. The dark photon scenario [64–69] has been extensively analyzed in the literature, and has also been the subject of many current experimental searches [54] (see [88] for a recent review on the dark photon physics).

Indeed, a dark photon can have renormalizable couplings to SM fields [64], induced by a tree-level kinetic mixing with an ordinary photon, namely $\epsilon\, F_{\mu\nu} F^{D}_{\mu\nu}$, where $F_{\mu\nu}$ and $F^{D}_{\mu\nu}$ are the field strengths of the photon and dark photon, respectively. The dimensionless mixing parameter ϵ is expected to depend only logarithmically on the UV scale. After diagonalizing the kinetic term, a massive dark photon can acquire a millicharged tree-level coupling to an ordinary SM charged particle, which is proportional to the ϵ parameter [64]. For dark photon masses above one MeV, the dark photon can then decay into SM charged leptons. Consequently, strong limits on the ϵ parameter for dark photon masses above one MeV have been set from direct di-lepton searches at colliders and fixed target experiments, as well as indirectly from supernovae [88].

On the other hand, for a massless dark photon things go in a different way. The kinetic mixing can be fully rotated away, and no tree-level coupling with charged SM fields is left. At the same time, a massless dark photon can potentially acquire couplings to SM fields via higher-dimensional operators [64]. This would make in general a massless dark photon search different from the massive case, and strongly dependent on the size of the

effective scale of the associated operator. On the other hand, the fine structure constant (α_D) characterizing the dark $U(1)_D$ interaction can be relatively large, presently missing relevant experimental constraints [88].

In this paper, we restrict our discussion of the dark photon production to Higgs-boson-mediated processes. The latter manifests crucial *non-decoupling* properties that makes the corresponding rates insensitive to the UV effective scale and controlled by the electroweak scale, just as in the one-loop photon–photon ($H\gamma\gamma$) or gluon–gluon (Hgg) Higgs SM amplitudes (for a review on more general Higgs couplings to the dark sector see [89]).

Indeed, both massless and massive dark photons can have effective couplings with the Higgs boson induced by the exchange of messenger fields [74,90]. For the Higgs coupling to a photon and a dark photon ($H\gamma\gamma_D$), the effective coupling is dominated by the dimension-five operator $HF_{\mu\nu}F^D_{\mu\nu}$. Remarkably, as observed in [74], this interaction manifests non-decoupling effects with respect to the UV theory in both massless and massive dark photon scenarios. In the massive case, the dark photon can also couple to the Higgs via top-quark and $W^\pm$ boson loops through millicharge effects (proportional to the ϵ parameter). On the other hand, the latter tends to be very much suppressed with respect to heavy-messenger loop-induced contributions due to the present strong ϵ bounds for a light dark photon [88]. Hence, dark photon production mediated by the Higgs boson via messenger loops is expected to be the leading dark photon production channel in both the massless and massive cases.

Using the minimal model of [74] as a (renormalizable) benchmark scenario, one can indeed show that the associated scale depends only on the Higgs vev, and it is independent on the UV scale set by the mass of the (heavy) messenger fields running in the loop. In particular, for a minimal scenario, this scale will depend on only two free dimensionless parameters, α_D and ξ—the mixing parameter in the scalar messenger sector defined in the following—which satisfies the condition $|\xi| < 1$.

The effective Higgs–dark-photon couplings can induce the visible Higgs decay into a photon plus a dark photon $H \to \gamma\gamma_D$. Since a massless γ_D is not detected, the corresponding signature at the LHC would be characterized by an almost monochromatic photon, with the energy half of the Higgs boson mass in its rest frame, plus missing transverse energy [91,92]. Due to the expected non-decoupling properties, this decay might have measurable rates and could be a golden channel for the massless dark photon discovery. Indeed, other dark photon production mechanisms at colliders are sensitive to the UV effective scale, being massless dark photons coupled in general via higher dimensional operators which do experience decoupling properties. Similar conclusions hold also for the Higgs coupling to two dark photons ($H\gamma_D\gamma_D$), which gives contribution to the invisible width of the Higgs boson.

The above features also characterize a massive but light dark photon, which is not decaying into visible particles inside the detector.

Experimental searches for the mono-photon Higgs signature have been recently carried out at the LHC by the ATLAS [93] and CMS [94,95] collaborations, for the most promising Higgs production channels of vector boson fusion (VBF) and associated vector boson production (VH). The negative result of these searches have been turned into a few percent upper bounds on the corresponding Higgs $H \to \gamma\gamma_D$ branching ratio (BR).

In this review, we will focus on the physics of the massless (or lightly massive) *invisible* dark photon, and its implications for the $H \to \gamma\gamma_D$ decay rates. We will analyze the main discovery signatures for this decay channel at the LHC [91,92] and future e^+e^- colliders [96,97], including a discussion on recent relevant ATLAS and CMS analyses [93–95].

With respect to previous reviews on dark photon phenomenology [88,89], a few relevant theoretical aspects underlying the dark photon connection to the Higgs boson sector have been scrutinized and discussed in detail. In particular, the relevant effective couplings of the Higgs boson to dark photon and photon (or Z boson) are explicitly shown at one loop by means of a simplified model for the dark sector. We also provide predictions for the corresponding new physics contributions to the decay channels $H \to \gamma\gamma$,

and $H \to 2\,gluons$. This will allow a model-independent analysis of the $H \to \gamma\gamma_D$ rate, satisfying all constraints arising from the LHC measurements of Higgs properties. Finally, based on general theoretical arguments, we will show how the detection of a hypothetical $H \to \gamma\gamma_D$ signature could set strong evidence for the spin-one nature of the dark photon, definitely disfavoring different-spin candidates giving rise to missing energy. We will also include a detailed analysis of the dark photon production mediated by the Higgs boson at future e^+e^- colliders, which has not been covered in [89].

The paper is organized as follows. In Section 2, we provide the theoretical description of leading Higgs couplings to a massless dark photon and the results for the corresponding Higgs decay BR's. We also stress the unique connection between a two-body $H \to \gamma\, X_{inv}$ signature and the production of a spin-one (dark photon) particle. In Section 3, we analyze the signal arising from the Higgs decay $H \to \gamma\gamma_D$ at the LHC in the main Higgs production channels of gluon–gluon fusion and VBF, also discussing the dominant backgrounds. In Section 4, most recent LHC experimental results on the $H \to \gamma\gamma_D$ searches by ATLAS and CMS collaborations are presented. Future perspectives for dark photon searches at future/possible LHC upgrades are also presented. In Section 5, Higgs-mediated dark photon production channels at future e^+e^- colliders are discussed, while our conclusions are given in Section 6.

2. Theoretical Framework

The dark photon is the quanta associated to an abelian $U(1)_D$ gauge symmetry of a hypothetical dark sector made up of particles completely neutral under the SM interactions. We will see there are actually two kinds of dark photons—massless or massive—whose theoretical characteristics as well as experimental signatures can be quite distinct.

Let us start by reviewing how the dark photon can couple with ordinary matter and gauge fields. There are different ways a dark photon can communicate with the ordinary world. The most known portal is provided assuming the existence of a tree-level *kinetic-mixing* term with ordinary photons in the Lagrangian, namely a term proportional to $\epsilon\, F_{\mu\nu}F^D_{\mu\nu}$, where $F_{\mu\nu}$ and $F^D_{\mu\nu}$ are the field strength of the photon and $U(1)_D$ the gauge field, respectively, being ϵ a small dimensionless parameter.

The physics arising from the kinetic mixing differs for a truly massless dark photon with respect to a massive one regardless of the latter mass size. For massless dark photons, one can rotate the fields in such a way that the dark photon becomes coupled at tree level only to the dark charged sector, while the dark charged matter fields also acquire a "milli" charge proportional to $\epsilon\, e_D$, where e_D is the $U(1)_D$ charge unit, and correspondingly mildly couples to an ordinary photon as well. On the other hand, in the massive case, the freedom of field rotation is prevented by the presence of the dark photon mass term in the Lagrangian [64,88]. Then, the massive dark photon field in general couples to both the $U(1)_D$ and SM electromagnetic currents (in the latter case with a "milli" charge coupling proportional to $\epsilon\, e$).

A different type of portal assumes the existence of (typically scalar or fermion) heavy messenger fields that are charged under both the SM and the $U(1)_D$ gauge sectors. The presence of a tree-level kinetic mixing at any scale is unavoidable in the presence of messenger fields. Indeed, even if a *tree-level* mixing term is assumed to vanish at some high energy scale, the radiative corrections could regenerate it at low energy scales. However, in the presence of messenger fields, the massless dark photon can acquire couplings to ordinary SM particles as well via higher dimensional operators that can be induced via loop effects.

In conclusion, following the above considerations, the physics of massless and massive dark photons can be summarized as follows:

- A massless dark photon does not couple at tree level to any of the SM currents and interacts instead with ordinary matter only through operators of dimension higher than four;

- A massive dark photon, in addition to higher dimensional operators as in the massless case, can couple to ordinary matter through a current (with an arbitrarily small charge) via a renormalizable operator of dimension four. The massless limit of this case does not correspond to the massless case above.

Because of their different coupling to SM particles, they are characterized by a different phenomenology.

Now we will focus on the phenomenology of a massless dark photon coupled to the Higgs field. The corresponding results can be easily generalized to a massive dark photon.

2.1. The Model

As benchmark model for the portal sector, we consider the scenario discussed in [91] for the radiative generation of the SM Yukawa couplings. The model assumes a generic messenger sector consisting of *left*-doublets (indicated with a "hat") and *right*-singlets of the $SU(2)_L$ gauge group, namely $\hat{S}_L^{U_i}$, $\hat{S}_L^{D_i}$ and $S_R^{U_i}$, $S_R^{D_i}$ scalars, respectively, for the colored messengers and analogous ones for the electroweak messengers $\hat{S}_L^{E_i}$, $\hat{S}_L^{N_i}$ and $S_R^{E_i}$, $S_R^{N_i}$, with a flavor universal mass term for each i, with generation index $i = 1, 2, 3$. Due to the fact that all messenger fields in [91] have universal Yukawa couplings to dark fermions and quarks/leptons (to radiatively generate the SM Yukawa couplings), they incidentally have the same SM quantum numbers (QN) as squarks and sleptons of (SUSY) models. Moreover, due to the fact that dark fermions are charged under $U(1)_D$, the messengers must also carry additional $U(1)_D$ charges. In Table 1, we report the corresponding QN for colored and EW messenger fields as given in [91].

Table 1. Gauge quantum numbers for the strongly-interacting (S^{D_i,U_i}) and EW color singlet (S^{E_i,N_i}) messenger fields, and scalar singlet S_0, with the $i = 1, 2, 3$ index associated to the SM fermion generations. $U(1)_D$ is the gauge symmetry in the dark sector. The electric charge (in e units) of each field is given by $Q = I_3 + \frac{Y}{2}$, where Y is the hypercharge and I_3 is the eigenvalue of the third weak isospin generator, while the dark $U(1)_D$ charges are in units of the fundamental dark charge e_D.

Fields	$SU(2)_L$ Repr.	$U(1)_Y$ Charge	$SU(3)_c$ Repr.	$U(1)_D$ Charge
$\hat{S}_L^{D_i}$	2	1/3	3	q_{D_i}
$\hat{S}_L^{U_i}$	2	1/3	3	q_{U_i}
$S_R^{D_i}$	1	−2/3	3	q_{D_i}
$S_R^{U_i}$	1	4/3	3	q_{U_i}
$\hat{S}_L^{E_i}$	2	−1	1	q_{E_i}
$\hat{S}_L^{N_i}$	2	−1	1	q_{N_i}
$S_R^{E_i}$	1	−1	1	q_{E_i}
$S_R^{N_i}$	1	0	1	q_{N_i}
S_0	1	0	1	0

Since we are interested in providing a minimal UV completion for the radiative generation of the effective Higgs boson couplings involving both dark photons and SM gauge bosons, here we restrict to only the interaction of messenger fields with couplings to the Higgs boson [91]. In particular, for the colored messengers sector (omitting the flavor and color indices) the interaction Lagrangian is

$$\mathcal{L}_{MS}^{I} = \lambda_S S_0 \left(\tilde{H}^\dagger S_L^U S_R^U + H^\dagger S_L^D S_R^D \right) + h.c., \quad (1)$$

where λ is a universal coupling, the doublet messenger fields components are $S_L^U = (S_L^{U_1}, S_L^{U_2})$, $S_L^D = (S_L^{D_1}, S_L^{D_2})$, and S_0 is a singlet scalar field that has a vev.

After the singlet S_0 scalar obtains a vev $\langle S_0 \rangle$, trilinear Higgs couplings to messenger fields are generated, and effective couplings of the Higgs to dark photons, $H\gamma\,\gamma_D$ and $H\gamma_D\gamma_D$, are induced at one-loop, and are proportional to the parameter $\mu_S \equiv \lambda_S \langle S_0 \rangle$. However, after the electroweak symmetry breaking (EWSB), a mixing mass term in the left and right messenger sectors arises, which is proportional to $\mu_S v$, being v the Higgs vev.

Then, focusing on the left and right messenger fields components, the free kinetic Lagrangian for a generic $S_{L,R}$ (for each U and D messenger sectors, and for the EW sector as well) is

$$\mathcal{L}_S^0 \;=\; \partial_\mu \hat{S}^\dagger \partial^\mu \hat{S} - \hat{S}^\dagger M_S^2 \hat{S}, \tag{2}$$

where $\hat{S} = (S_L, S_R)$ (omitting both U, D and flavor indices, and also $SU(2)_L$ indices), and the mass term is given by

$$M_S^2 = \begin{pmatrix} m_L^2 & \Delta \\ \Delta & m_R^2 \end{pmatrix}, \tag{3}$$

with $\Delta = \mu_S v$ parametrising the scalar left-right mixing. It is understood that each term inside Equation (3) is proportional to the 3×3 unity matrix in the flavor space. According to the minimal flavor violation hypothesis [98], flavor universality for the m_L^2 and m_R^2 mass terms is assumed. Then, for each flavor sector, the 2×2 matrix of Equation (3) can be diagonalized by the matrix

$$U = \begin{pmatrix} \cos\theta & \sin\theta \\ -\sin\theta & \cos\theta \end{pmatrix}, \tag{4}$$

where $\tan\theta = 2\Delta/(m_L^2 - m_R^2)$, with mass eingenvalues $m_\pm^2 = \bar{m}^2 \pm \Delta/\sin 2\theta$, and $\bar{m}^2 = (m_L^2 + m_R^2)/2$ being the average mass squared.

Concerning the dark photon interaction with the messenger fields, it can be simply obtained by substituting the partial derivative ∂_μ with the covariant derivative $D^\mu = \partial^\mu + ie_D q A_D^\mu$ in the kinetic term of messenger fields in Equation (2), where A_D^μ is the dark photon field, e_D stands for the unit of $U(1)_D$ charge, and q is the corresponding charge eigenvalue of the field to which the covariant derivative applies. Notice that, after rotating the messenger fields to the corresponding mass eigenstates basis, the interaction Lagrangian ($\mathcal{L}_S^{\rm DP}$) involving messenger fields and dark photon remains diagonal in the mass eigenstate basis. Indeed, the messenger fields $\hat{S} = (S_L, S_R)$ subject to the rotation have the same $U(1)_D$ charge, namely

$$\mathcal{L}_S^{\rm DP} \;=\; (D_\mu \hat{S}_{\rm M})^\dagger (D^\mu \hat{S}_{\rm M})\,, \tag{5}$$

where $\hat{S}_{\rm M} = (S_1, S_2)$ symbolically indicates the messenger mass eigenstates (with the U, D and flavor indices omitted).

Finally, notice that since all messenger fields are charged under $U(1)_D$ interactions, no mixing among the Higgs field and electroweak messenger fields can arise [assuming $U(1)_D$ is unbroken] due to $U(1)_D$ gauge invariance or charge conservation.

2.2. The Higgs Decay $H \to \gamma\gamma_D$

After the EWSB, the interaction in Equation (1) can generate the Higgs boson decay into a photon plus a dark photon

$$H \to \gamma\gamma_D\,, \tag{6}$$

whose Feynman diagrams are reported in Figure 1.

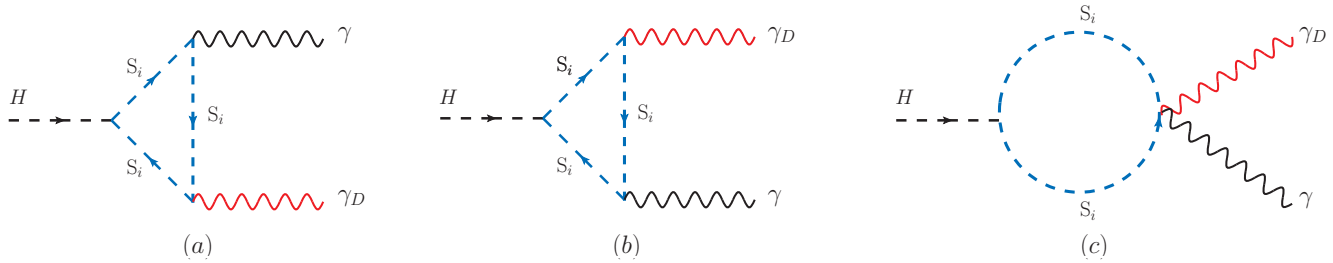

Figure 1. Feynman diagrams (**a**–**c**) contributing to the $H \to \gamma\gamma_D$ decay amplitude, where γ and γ_D are the photon and dark photon, respectively. The dashed blue lines stand for the mass eigenstates (S_i) of messenger scalar fields running in the loop.

If we define $\varepsilon_1^\mu(k_1)$ and $\varepsilon_2^\mu(k_2)$ the photon and dark photon polarization vectors, respectively, we can express the $H \to \gamma\,\gamma_D$ amplitude as

$$M_{\gamma\gamma_D} \;=\; \frac{1}{\Lambda_{\gamma\gamma_D}}\, T_{\mu\nu}(k_1,k_2)\varepsilon_1^\mu(k_1)\varepsilon_2^\nu(k_2), \tag{7}$$

where $\Lambda_{\gamma\gamma_D}$ parametrizes the effective scale associated to the NP, and the tensor $T^{\mu\nu}$ is given by

$$T^{\mu\nu}(k_1,k_2) \equiv g^{\mu\nu}k_1\cdot k_2 - k_2^\mu k_1^\nu\,, \tag{8}$$

where k_1 and k_2 are the photon and dark photon four-momenta, respectively, satisfying the on-shell conditions $k_1^2 = k_2^2 = 0$. It is easy to verify that the $M_{\gamma\gamma_D}$ amplitude is gauge invariant due to the Ward identities $k_1^\mu T_{\mu\nu}(k_1,k_2) = k_2^\nu T_{\mu\nu}(k_1,k_2) = 0$. The total width is then

$$\Gamma(H\to\gamma\gamma_D) = \frac{m_H^3}{32\,\pi\,\Lambda^2_{\gamma\gamma_D}}\,, \tag{9}$$

with m_H the Higgs boson mass. To compute the $\Lambda_{\gamma\gamma_D}$ scale, we compute the Feynman diagrams in Figure 1, and match the resulting amplitude with the expression in Equation (7). If we neglect the Higgs boson mass with respect to the messenger masses $m_{L,R}$ in the loop, we obtain

$$\frac{1}{\Lambda_{\gamma\gamma_D}} \;=\; \frac{\mu_S\sqrt{\alpha\alpha_D}R}{12\pi}\left(\frac{\sqrt{(m_L^2-m_R^2)^2+4\Delta^2}}{m_L^2m_R^2-\Delta^2}\right)\sin 2\theta, \tag{10}$$

where $R = N_c\sum_{i=1}^3(e_U q_{U_i} + e_D q_{D_i})$, with q_{U_i}, q_{D_i} the $U(1)_D$ charges in the up and down sectors, and $e_U = \frac{2}{3}$, $e_D = -\frac{1}{3}$ the corresponding EM charges; α is the EM fine structure constant, $N_c = 3$ is the number of colors, and θ is the mixing angle diagonalizing Equation (3). The above result can be easily generalized to include the contributions of messengers in the leptonic sector, whose contribution is $R = e_E\sum_{i=1}^3(q_{E_i})$, since in this case $N_c = 1$, $e_U = 0$, and $e_D = -1$.

A minimal scenario can be realized if we further assume mass universality in the S_L and S_R messenger sector, with in particular $m_L \simeq m_R \equiv \bar{m}$. Correspondingly, the mixing angle is set to $\theta = \pi/4$. Then, by defining the mixing parameter $\xi = \Delta/\bar{m}^2$, the eigenvalues of Equation (3) become $m_\pm^2 = \bar{m}^2(1\pm\xi)$, and the $\Lambda_{\gamma\gamma_D}$ scale simplifies to

$$\Lambda_{\gamma\gamma_D} \;=\; \frac{6\pi v}{R\sqrt{\alpha\alpha_D}}\frac{1-\xi^2}{\xi^2}\,. \tag{11}$$

To avoid tachyons, the mixing parameter should be in the range $0 \le \xi \le 1$. However, the upper limit $\xi = 1$ is not quite realistic, corresponding to a massless messenger eigenvalue.

A viable upper limit on ξ can be obtained by requiring that the lightest colored messenger mass satisfies the current lower limit from negative searches of colored scalar fields at the LHC that we will name m_B. In particular, by imposing $m_-^2 > m_B^2$, one obtains the constraint $\xi < 1 - \frac{m_B^2}{\bar{m}^2}$.

One remarkable aspect of the result in Equation (11) is the non-decoupling that can show up in the $H \to \gamma\gamma_D$ decay for increasing messenger masses, similar to the $H \to \gamma\gamma$ decay in the SM in the limit of large top-quark and $W^\pm$ masses. In fact, $\Lambda_{\gamma\gamma_D}$ in Equation (11) effectively depends only on one mass scale, i.e., the Higgs vev (as in the SM two-photon channel), multiplied by a function of two dimensionless free parameters: the mixing parameter ξ and the dark fine structure constant α_D. Both parameters can be in principle moderately large (although smaller than one), regardless of the scale set by the average messenger mass $\bar{m}$. A non-decoupling limit is then realised in the UV regime in which the two mass eigenvalues $m_\pm^2$ in the left and right messenger sectors become arbitrarily large, while keeping fixed (and finite) their relative splitting, expressed by the ξ parameter. This can indeed occur since the mixing term $\xi = \mu_S v/\bar{m}^2$ actually depends on two independent mass parameters, the μ_S scale and the average messenger mass $\bar{m}$. Hence, keeping ξ finite at large mass scales requires the μ_S term to scale as $\bar{m}^2/v$ for large $\bar{m}$. This non-decoupling regime is for instance naturally realized in the model proposed in [74]—on which the simplified dark sector model assumed here is inspired—where all the SM Yukawa couplings are radiatively generated by a dark sector. On the other hand, as stressed in [91], non-decoupling is a general property of the Higgs boson and does not depend on the peculiar structure of the model in [74], provided a messenger sector connecting the SM and the dark sector exists.

The messenger interactions can similarly induce new one-loop contributions to the Higgs decay $H \to \gamma\gamma$ and to the invisible channel $H \to \gamma_D\gamma_D$ arising from decays into two dark photons.

The corresponding amplitudes have the same structure as in Equation (7), and we obtain

$$\Lambda_{\gamma\gamma} = \Lambda_{\gamma\gamma_D}\frac{R}{R_0}\sqrt{\frac{\alpha_D}{\alpha}}, \quad \Lambda_{\gamma_D\gamma_D} = \Lambda_{\gamma\gamma_D}\sqrt{\frac{\alpha}{\alpha_D}}\frac{R}{R_1}, \tag{12}$$

where $R_0 = 3N_c(e_U^2 + e_D^2)$, and $R_1 = N_c\sum_{i=1}^3\left(q_{U_i}^2 + q_{D_i}^2\right)$, showing analogous non-decoupling properties.

Similar contributions are induced at one loop for the Higgs decay $H \to Z\gamma_D$, and for the two-gluon channel $H \to gg$.

When messengers are much heavier than the Higgs boson, the low-energy Higgs dark photon interactions can be described by the formalism of effective Lagrangians. By retaining only the relevant low-energy operators, the corresponding Lagrangian $\mathcal{L}_{\mathrm{DP_H}}$ can then be expressed in terms of (real) dimensionless coefficients C_{ij} (with $i, j = \gamma_D, \gamma, Z, g$) as

$$\mathcal{L}_{\mathrm{DP_H}} \simeq \frac{\alpha}{\pi}\left(\frac{C_{\gamma\gamma_D}}{v}F^{\mu\nu}F^D_{\mu\nu}H + \frac{C_{Z\gamma_D}}{v}Z^{\mu\nu}F^D_{\mu\nu}H + \frac{C_{\gamma_D\gamma_D}}{v}F^{D\mu\nu}F^D_{\mu\nu}H\right), \tag{13}$$

where α is the SM fine structure constant, and $F_{\mu\nu}$, $Z_{\mu\nu}$, $F^D_{\mu\nu}$ are the photon, Z-boson, and dark photon field strengths, respectively ($F_{\mu\nu} \equiv \partial_\mu A_\nu - \partial_\nu A_\mu$ for the photon field, A_μ, and analogously for $F^D_{\mu\nu}$ and $Z_{\mu\nu}$).

Additional contributions are induced to the SM Higgs effective interactions with two photons, one photon and a Z, and two gluons that can be absorbed into the effective Lagrangian $\mathcal{L}_{\mathrm{SM_H}}$ given by

$$\mathcal{L}_{\mathrm{SM_H}} \simeq \frac{\alpha}{\pi}\left(\frac{C_{\gamma\gamma}}{v}F^{\mu\nu}F_{\mu\nu}H + \frac{C_{Z\gamma}}{v}Z^{\mu\nu}F_{\mu\nu}H\right) + \frac{\alpha_S}{\pi}\frac{C_{gg}}{v}G^{a\mu\nu}G^a_{\mu\nu}H, \tag{14}$$

where α_S is the SM strong coupling constant, $G^a_{\mu\nu}$ stands for the gluon field strength, and a sum over the color index a is understood. Then, for the C_{ij} coefficients one finds

$$\begin{aligned}
C_{\gamma\gamma_D} &= \sqrt{\frac{\alpha_D}{\alpha}} \sum_{i=q,l} \frac{R_1^i}{12} \frac{\xi_i^2}{1-\xi_i^2}\,, \\
C_{\gamma_D\gamma_D} &= \frac{\alpha_D}{\alpha} \sum_{i=q,l} \frac{R_2^i}{12} \frac{\xi_i^2}{1-\xi_i^2}\,, \\
C_{Z\gamma_D} &= \sqrt{\frac{\alpha_D}{\alpha}} \sum_{i=q,l} R^i_{Z\gamma} \frac{R_1^i}{12} \frac{\xi_i^2}{1-\xi_i^2}\,, \\
C_{\gamma\gamma} &= C^{\rm SM}_{\gamma\gamma}\left(1+\chi \sum_{i=q,l} \frac{R_0^i \xi_i^2}{3F\left(1-\xi_i^2\right)}\right), \\
C_{Z\gamma} &= C^{\rm SM}_{Z\gamma}\left(1+\chi \sum_{i=q,l} R^i_{Z\gamma} \frac{R_0^i \xi_i^2}{3F\left(1-\xi_i^2\right)}\right), \\
C_{gg} &= C^{\rm SM}_{gg}\left(1-\chi \frac{\xi_q^2}{3F_q\left(1-\xi_q^2\right)}\right),
\end{aligned} \tag{15}$$

where $C^{\rm SM}_{\gamma\gamma} = \frac{1}{8}F$, $C^{\rm SM}_{gg} = \frac{1}{16}F_q$, and the constants $R^{q,l}_{0,1,2}$ are given by

$$\begin{aligned}
&R_0^q = 3N_c(e_U^2+e_D^2), && R_0^l = 3\,e_E^2\,, \\
&R_1^q = N_c \sum_{i=1}^{3}\left(e_U q_{U_i} + e_D q_{D_i}\right), && R_1^l = e_E \sum_{i=1}^{3}\left(q_{E_i}\right), \\
&R_2^q = N_c \sum_{i=1}^{3}\left(q_{U_i}^2 + q_{D_i}^2\right), && R_2^l = \sum_{i=1}^{3}\left(q_{E_i}^2 + q_{N_i}^2\right),
\end{aligned} \tag{16}$$

with $e_U = 2/3$, $e_D = -1/3$, and $e_E = -1$, the electric charges for up-, down-quarks, and charged leptons, respectively, while q_i are the corresponding $U(1)_D$ charges as defined in Table 1. Here F, F_F, and F_q are the usual SM loop factors given by

$$F = F_W(\beta_W) + F_F\,, \qquad F_F = \sum_f N_c Q_f^2 F_f(\beta_f)\,, \qquad F_q = \sum_f F_f(\beta_f)\,, \tag{17}$$

with $N_c = 1(3)$ for leptons (quarks), respectively, $\beta_W = 4m_W^2/m_H^2$, $\beta_f = 4m_f^2/m_H^2$, and

$$F_W(x) = 2 + 3x + 3x(2-x)f(x)\,, \qquad F_f(x) = -2x(1+(1-x)f(x))\,, \tag{18}$$

where $f(x) = \arcsin^2[\frac{1}{\sqrt{x}}]$, for $x \geq 1$, and $f(x) = -\frac{1}{4}\left(\log\left(\frac{1+\sqrt{1-x}}{1-\sqrt{1-x}}\right) - i\pi\right)^2$, for $x < 1$. Including only the $W^\pm$ and top-quark loops in F, we obtain, for $m_H = 125$ GeV, $F \simeq 6.5$, $F_t \simeq -1.38$. The coefficient $\chi = \pm 1$ in Equation (16) parametrizes the relative sign of the NP and SM contributions in the amplitudes of the $H \to \gamma\gamma$ and $H \to gg$ decays. In our model, the χ sign is a free parameter since it is related to the relative sign of the SM Higgs vev and the S vev. [Due to the Bose statistics of the scalar messenger fields, the relative sign of the messenger contributions to $C_{\gamma\gamma}$ (or $C_{Z\gamma}$) and C_{gg} is anyhow predicted to be negative, as can be checked in Equation (16)].

Concerning the value of the $R^{q,l}_{Z\gamma}$ constants in Equation (16), this is discussed in more detail in [96]. In the case of a pair of mass-degenerate down- and up-type colored messengers running in the loop and in the limit of small mixing, one has $R^q_{Z\gamma} \simeq 0.79$, while for a pair of mass-degenerate EW messengers one has $R^l_{Z\gamma} \simeq 0.045$.

Notice that, due to the fact that $\xi_i^2 \propto v^2$, all the Wilson coefficients in front of the operators in Equations (13) and (14) vanish in the limit of $v \to 0$. This is due to gauge invariance. Indeed, the corresponding SM gauge-invariant effective Lagrangians above the EW scale must require dimension six operators, which are obtained by replacing the Higgs field H with $H \to \hat{H}^\dagger \hat{H}$ in Equations (13) and (14), where $\hat{H}$ is the $SU(2)$ Higgs doublet. Then, after the Higgs field obtains the vev, the Lagrangians in Equations (13) and (14) are obtained, with associated Wilson coefficients proportional to v.

Finally, by taking into account the parametrization in Equations (13) and (14), one has for the $H \to \gamma\gamma_D$ and $H \to gg$ decay widths [91]

$$\Gamma(H \to \gamma\gamma_D) = \frac{m_H^3 \alpha^2 |C_{\gamma\gamma_D}|^2}{8\pi^3 v^2}, \quad \Gamma(H \to gg) = \frac{m_H^3 \alpha_S^2 |C_{gg}|^2 (N_c^2 - 1)}{4\pi^3 v^2}, \tag{19}$$

where $N_c = 3$ and $\Gamma(H \to gg)$ is understood to be inclusive in gluons final states. Analogous results can be obtained for the $H \to \gamma_D\gamma_D$, $H \to Z\gamma_D$, $H \to \gamma\gamma$ widths replacing $|C_{\gamma\gamma_D}|^2$ by $2|C_{\gamma_D\gamma_D}|^2$, $|C_{Z\gamma_D}|^2$, $2|C_{\gamma\gamma}|^2$, respectively.

It is also useful to express the BR's for $H \to \gamma\gamma_D$, $\gamma_D\gamma_D$, $\gamma\gamma$ as a function of the *relative* exotic NP contribution r_{ij} to the $H \to ij$ decay width, as the ratio

$$r_{ij} \equiv \frac{\Gamma_{ij}^{\rm m}}{\Gamma_{\gamma\gamma}^{\rm SM}}, \tag{20}$$

with $\Gamma_{ij}^{\rm m}$ generically indicating the pure messenger contribution to $H \to ij$, with $i, j = \gamma, \gamma_D$. Analogously, the *relative* deviation for the $H \to gg$ decay width will be defined as

$$r_{gg} \equiv \frac{\Gamma_{gg}^{\rm m}}{\Gamma_{gg}^{\rm SM}}. \tag{21}$$

Then, one obtains the following model-independent parametrization of the $H \to \gamma\gamma_D$, $\gamma_D\gamma_D$, $\gamma\gamma$ BR's as functions of r_{ij} [91]

$$\begin{aligned} {\rm BR}_{\gamma\gamma_D} &= {\rm BR}_{\gamma\gamma}^{\rm SM} \frac{r_{\gamma\gamma_D}}{1 + r_{\gamma_D\gamma_D} {\rm BR}_{\gamma\gamma}^{\rm SM}}, \\ {\rm BR}_{\gamma_D\gamma_D} &= {\rm BR}_{\gamma\gamma}^{\rm SM} \frac{r_{\gamma_D\gamma_D}}{1 + r_{\gamma_D\gamma_D} {\rm BR}_{\gamma\gamma}^{\rm SM}}, \\ {\rm BR}_{\gamma\gamma} &= {\rm BR}_{\gamma\gamma}^{\rm SM} \frac{\left(1 + \chi\sqrt{r_{\gamma\gamma}}\right)^2}{1 + r_{\gamma_D\gamma_D} {\rm BR}_{\gamma\gamma}^{\rm SM}}, \end{aligned} \tag{22}$$

where as in Equation (16), $\chi = \pm 1$ parametrizes the relative sign of the SM and exotic NP amplitudes, and ${\rm BR}_{ij}$ stands for ${\rm BR}(H \to ij)$. As a first approximation, to simplify the analysis, we have neglected in Equation (23) the r_{gg} and $r_{\gamma\gamma}$ contributions to the total width of the Higgs since they are expected to be negligible.

Concerning the Higgs production at the LHC, if colored messenger fields are involved, the cross section from the gluon–gluon fusion modifies as follows

$$\sigma_{gg\to H} = \sigma_{gg\to H}^{SM} \left(1 - \chi\sqrt{r_{gg}}\right)^2. \tag{23}$$

This correction should be taken into account for the colored messengers contribution to the Higgs production from gluon–gluon fusion. In particular, the signal strength $R_{\gamma\gamma} = \frac{\sigma_{gg\to H} {\rm BR}_{\gamma\gamma}}{\sigma_{gg\to H}^{\rm SM} {\rm BR}_{\gamma\gamma}^{\rm SM}}$, will be given by

$$R_{\gamma\gamma} = \frac{{\rm BR}_{\gamma\gamma}}{{\rm BR}_{\gamma\gamma}^{\rm SM}} \left(1 - \chi\sqrt{r_{gg}}\right)^2. \tag{24}$$

The model predictions for the ratios r_{ij} $(i,j = \gamma, \gamma_D)$ as defined in Equation (20) [entering the model-independent BR's parametrization in Equation (23)], and r_{gg} as defined in Equation (21) are then given by

$$r_{\gamma\gamma_D} = 2\left(\sum_{i=l,q} X_i R_1^i\right)^2 \left(\frac{\alpha_D}{\alpha}\right), \quad r_{\gamma_D\gamma_D} = \left(\sum_{i=l,q} X_i R_2^i\right)^2 \left(\frac{\alpha_D}{\alpha}\right)^2, \tag{25}$$

$$r_{\gamma\gamma} = \left(\sum_{i=l,q} X_i R_0^i\right)^2, \qquad r_{gg} = \frac{X_q^2 F^2}{F_q^2}, \tag{26}$$

where the extra factor two in $r_{\gamma\gamma_D}$ comes from statistics and

$$X_{l(q)} \equiv \frac{\xi_{l(q)}^2}{3F(1-\xi_{l(q)}^2)}, \tag{27}$$

with $R_{0,1,2}^{q,l}$ defined in Equation (17).

Following the analysis in [91], we now consider a minimal model with only one (colorless) messenger contributing with unit charges $e = q = 1$. Updated predictions of this scenario with respect to [91] are reported in Figure 2, where we plot $\mathrm{BR}(H \to \gamma\gamma_D)$ versus α_D. The curves are evaluated for $r_{\gamma\gamma} = 0.01,\ 0.05\,, 0.1\,, 0.15$, corresponding to mixing parameter $\xi = 0.81, 0.90, 0.92, 0.94$, respectively. The red squares correspond to different $\mathrm{BR}_{\gamma_D\gamma_D}$ values (increasing from left to right), with the $H \to \gamma_D\gamma_D$ decay assumed to provide the leading contribution to the Higgs invisible branching ratio $\mathrm{BR}_{\mathrm{inv}}$. The value $\mathrm{BR}_{\mathrm{inv}} = 0.18$ correspond to the current experimental upper bound at 95% C.L. from CMS [99], which is less stringent than the corresponding one from ATLAS [100] ($\mathrm{BR}_{\mathrm{inv}} < 0.14$). Then, the points to the right of the red square with $\mathrm{BR}_{\mathrm{inv}} = 0.18$ can be assumed (conservatively) to be excluded at 95% C.L. from the current limits on $\mathrm{BR}_{\mathrm{inv}}$.

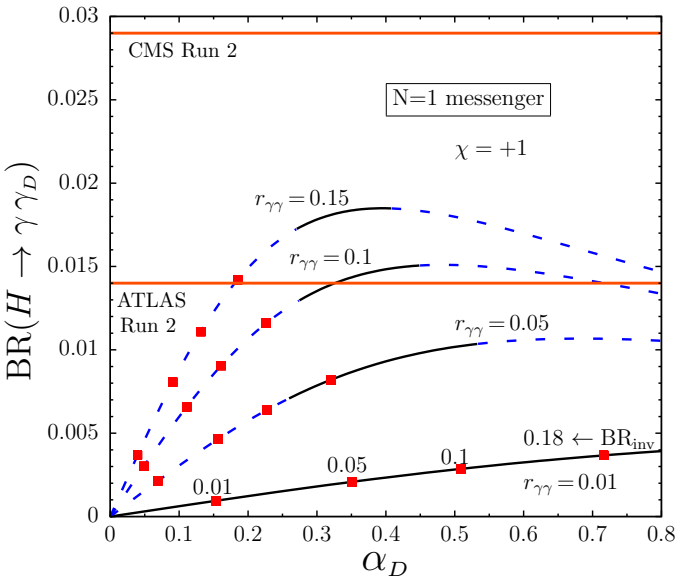

Figure 2. Predictions for $\mathrm{BR}(H \to \gamma\gamma_D)$ versus α_D for different $\mathrm{BR}_{\mathrm{inv}}$ and $r_{\gamma\gamma}$, for the minimal model of one (colorless) messenger with unit charges $e = q = 1$, and interference coefficient $\chi = +1$. Continuous (dashed) curves are allowed (excluded) by the $\mathrm{BR}(H \to \gamma\gamma)$ measurement at 2σ level. Horizontal lines indicate the corresponding ATLAS and CMS upper limits on $\mathrm{BR}(H \to \gamma\gamma_D)$ at 95% CL.

The full lines in Figure 2 correspond to the allowed values of $\mathrm{BR}_{\gamma\gamma}$ from the current limits on signal strengths at 2σ level [101]

$$0.93 \ \leq R_{\gamma\gamma} \leq 1.31\,, \tag{28}$$

while the dashed lines correspond to predictions outside that range. For the SM central value, we used $\mathrm{BR}^{\mathrm{SM}}_{\gamma\gamma} = 2.27 \times 10^{-3}$ [101]. The horizontal (orange) bands are the observed upper limit on $\mathrm{BR}_{\gamma\gamma_D}$ at 95% C.L. from the ATLAS (1.4%) [93] and CMS (2.9%) [94] analyses (these limits will be discussed in more detail in Section 4.2). We assume constructive interference between exotic and SM contributions (i.e., $\chi = 1$). Due to the asymmetry of the range in Equation (28) with respect to the $R_{\gamma\gamma}$ SM value, the experimental $\mathrm{BR}_{\gamma\gamma}$ constraints are correspondingly less effective, thus allowing a wider $\mathrm{BR}_{\gamma\gamma_D}$ range.

In Figure 3, we show the corresponding results, for a non-minimal model consisting of N=6 EW messengers [$SU(3)_c$ color singlet] (left plot), and a $SU(3)_c$ color triplet (right plot), with SM QN as in Table 1, and universal unitary $U(1)_D$ charges ($q_{E_i} = q_{N_i} = q_{D_i} = q_{U_i} = 1$) for all messengers. The same notations as in Figure 2 for the curves and red square points are adopted. Constructive interferences between exotic and SM contributions are assumed ($\chi = 1$). Curves are shown for $r_{\gamma\gamma} = 0.005, 0.02, 0.05, 0.1$, corresponding to universal mixing parameters $\xi^l = 0.56, 0.69, 0.76, 0.82$, and $\xi^q = 0.47, 0.60, 0.68, 0.74$, in the left and right plot, respectively. Note that, in Figure 3 (right plot), the $\mathrm{BR}_{\gamma\gamma}$ constraints take into account the messenger contribution to the gluon–gluon Higgs production cross section in the signal strength $R_{\gamma\gamma}$.

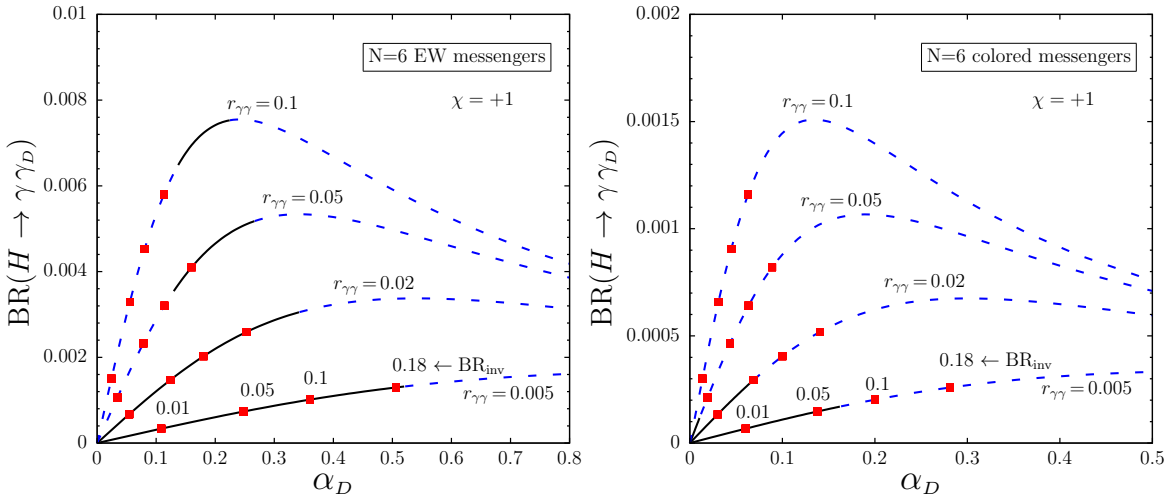

Figure 3. Predictions for $\mathrm{BR}(H \to \gamma\gamma_D)$ versus α_D, as in Figure 2, for extended portal models with N=6 EW $SU(3)_c$ singlet messengers (**left plot**) and N=6 $SU(3)_c$ triplet messengers (**right plot**), with the same SM QN of squarks and sleptons, and interference coefficient $\chi = +1$.

As we can see from these results, the allowed $\mathrm{BR}(H \to \gamma\gamma_D)$ for the minimal model is below 1%, consistently with all model parameters and current LHC constraints. On the other hand, the allowed $\mathrm{BR}(H \to \gamma\gamma_D)$ is reduced to less than 4×10^{-3} and 3×10^{-4} for the case of N=6 EW and colored messengers, respectively. Indeed, increasing the number of messengers at fixed $r_{\gamma\gamma}$, $\mathrm{BR}(H \to \gamma\gamma_D)$ decreases, since the larger the number of messengers the larger the contribution to the invisible rate given by $H \to \gamma_D\gamma_D$ in Equation (23), thus raising the total width and lowering $\mathrm{BR}(H \to \gamma\gamma_D)$.

A major result of this analysis is that the current sensitivity in the $\mathrm{BR}(H \to \gamma\gamma_D)$ measurement by ATLAS and CMS is presently almost one order of magnitude weaker than what is needed for detecting $\mathrm{BR}(H \to \gamma\gamma_D)$ in the allowed range, which is consistent with actual constraints on $\mathrm{BR}(H \to \gamma\gamma)$ and $\mathrm{BR}(H \to \text{invisible})$. The present SM agreement of the latter measurements indicates that more Higgs data are needed to explore the allowed $\mathrm{BR}(H \to \gamma\gamma_D)$ range at a few permil levels.

2.3. About the Spin of the Invisible Dark Photon

We now investigate whether the observation of the monochromatic photon signature discussed above could uniquely identify the dark photon production. Because of the isotropic nature of a scalar decay, in the $H \to \gamma X$ channel it is not possible to disentangle the spin nature of a dark X *boson* if X is detected as missing energy (note that a *fermionic* X particle would violate Lorentz invariance). Indeed, in the latter case, one cannot reconstruct X spin properties via kinematics of its visible decay products as in visible decays. Actually, we will see that that identification of such a signature with a dark *photon* (hence with a spin = 1 field) is the most realistic. In particular, below we will discuss possible scenarios of NP that could fake the dark photon signature, estimate their corresponding BR, and find that the dark photon $H \to \gamma\gamma_D$ interpretation of the $H \to \gamma X$ decay is by far the *most viable*.

Let us start with the possibility that the X particle is either a scalar or a pseudo-scalar particle (for instance, an axion-like particle). According to the angular momentum conservation, the Higgs boson cannot decay into a photon plus a scalar or pseudo-scalar particle, ruling out the possibility that X is a scalar or an axion-like particle. Indeed, by considering the two-body $H \to \gamma X$ decay in the rest frame of the Higgs boson, one can see that the (zero) helicity of the initial state cannot be conserved in the final state, due to the photon $h = \pm 1$ helicity, for scalar/pseudoscalar X's. This is also manifest in the effective Lagrangian approach when trying to build a gauge invariant $HS\gamma$ interaction (S standing for a generic scalar or pseudoscalar field). Indeed, this kind of interaction always vanishes for on-shell fields up to a total derivative. In particular, the Lagrangian is proportional to the following Lorentz and gauge invariant term $(\partial_\mu H)(\partial_\nu S)F^{\mu\nu}$, which is equivalent (up to a total derivative) to the sum of the $(\partial_\mu\partial_\nu H)SF^{\mu\nu}$ and $(\partial_\mu H)S\partial_\nu F^{\mu\nu}$ terms. The first term vanishes for the antisymmetric property of the $F^{\mu\nu}$ tensor under the (μ, ν) indices exchange, while the second term vanishes for on-shell photon fields due to the condition $\partial_\nu F^{\mu\nu} = 0$. Analogous conclusions hold for other terms with different combination of derivatives.

As a next potential candidate for the X boson in the $H \to \gamma X$ decay, we consider a massive spin-two field $X = G$ which is universally coupled to the total energy-momentum $T_{\mu\nu}$ of SM fields and of any potential NP beyond it. This is characterized by a rank-two symmetric and traceless tensor field $G_{\mu\nu}$ associated to the spin-two particle. As in the case of a massive graviton, this coupling reads

$$L_G = -\frac{1}{\Lambda_G} T^{\mu\nu} G_{\mu\nu} \,. \tag{29}$$

Since we assume $G_{\mu\nu}$ not to be related to gravitational interactions, we take the effective scale Λ_G as a free parameter, uncorrelated with the Planck mass, and of the order of the TeV scale. This scale turns to the well known $\Lambda_G^{-1} = \sqrt{8\pi G_N}$ in the ordinary case of a massless graviton in the General Relativity, with G_N the Newton constant [We do not make any hypothesis on the origin of such spin-two field, limiting ourselves to the linear theory in flat space, avoiding to enter into the issue of a consistent theory of massive spin-two fields related to the non-linear massive graviton interactions, since these do not affect the results presented here]. The free Lagrangian for the massive spin-two is then given by the Fierz–Pauli Lagrangian [102]. The corresponding Feynman rules for the G interaction in Equation (29) can be derived, for instance, from literature on quantum gravity models in large extra-dimensions where massive Kaluza–Klein graviton fields appear [103,104].

The coupling in Equation (29) is sufficient to generate new finite contributions at loop level for the effective $HG\gamma$ coupling entering the $H \to \gamma\, G$ decay. Indeed, due to the fact that $G_{\mu\nu}$ is coupled to the conserved energy momentum tensor $T^{\mu\nu}$ of matter fields, the theory is renormalizable against radiative corrections of SM matter fields only, provided $G_{\mu\nu}$ is taken as an external on-shell field.

From basic kinematical considerations, $H \to \gamma\, G$ is now allowed by angular momentum conservation, since a massive spin-two particle has five spin components, corresponding to $S_z = -2, -1, 0, 1, 2$ (with S_z standing for the usual eigenvalues of the spin component along the z-axis). However, only the $h = \pm 1$ helicity states of the massive

spin-two components will contribute to the decay. On the other hand, for a massless spin-two field (such as the Einstein graviton) the reaction is forbidden since the graviton has only two helicity states $h = \pm 2$, and the corresponding decay amplitude will vanish. Since the massless limit for the amplitude should be recovered from the massive spin-two case for vanishing masses, the rate of the $H \to \gamma\, G$ is expected to be suppressed by terms of the order of m_G^2/m_H^2.

To check these expectations, below we provide the most general Lorentz and gauge invariant structure of the $M(H \to \gamma\, G)$ amplitude for the decay

$$H \to \gamma(k)\, G(q) \tag{30}$$

that, to our knowledge, is not yet present in the literature and can be expressed as

$$M(H \to \gamma\, G) \;\; = \;\; \hat{M}_{\mu\alpha\beta}(p,q)\, \epsilon^{\mu}(k)\, \epsilon^{\alpha\beta}(q)\,. \tag{31}$$

Here $\epsilon^{\mu}(k)$ and $\epsilon^{\alpha\beta}(q)$ are the corresponding polarization vectors for the on-shell photon and massive graviton G, respectively, with $\epsilon^{\alpha\beta}(q)$ a symmetric and traceless spin-two tensor, satisfying the on-shell conditions $g_{\alpha\beta}\epsilon^{\alpha\beta}(q) = q_{\alpha}\epsilon^{\alpha\beta}(q) = q_{\beta}\epsilon^{\alpha\beta}(q) = 0$, with $g_{\mu\nu}$ the Minkowski metric. Then $\hat{M}_{\mu\alpha\beta}(p,q)$ can be parametrized as follows

$$\hat{M}_{\mu\alpha\beta}(p,q) \;\; = \;\; F_G\left[q_{\mu}\left(k_{\alpha}q_{\beta} + k_{\beta}q_{\alpha}\right) - 2\left(\frac{m_G^2}{k\cdot q}\right)q_{\mu}k_{\alpha}k_{\beta} + \left(m_G^2 - k\cdot q\right)\left(g_{\mu\alpha}k_{\beta} + g_{\mu\beta}k_{\alpha}\right)\right], \tag{32}$$

where F_G is a form factor having $[\text{mass}]^{-2}$ dimension (which absorbs also the electromagnetic couplings), depending only on the Higgs mass and m_G. The F_G form factor, which is expected to arise at loop level from the interaction in Equation (29) (see below), is free from power $m_G \to 0$ infrared singularities of the type $1/m_G^2$, since no G field is propagating in the loop.

It is easy to see that $\hat{M}_{\mu\alpha\beta}(p,q)$ in Equation (32) satisfies the following Ward Identities (WI)

$$k^{\mu}\hat{M}_{\mu\alpha\beta}(p,q) \;\; = \;\; q^{\alpha}\hat{M}_{\mu\alpha\beta}(p,q) \;=\; q^{\beta}\hat{M}_{\mu\alpha\beta}(p,q) \;=\; 0\,, \tag{33}$$

including the (traceless) additional condition $g^{\alpha\beta}\hat{M}_{\mu\alpha\beta}(p,q) = 2F_G k_{\mu}$ that vanishes when contracted with $\epsilon^{\mu}(k)$ for on-shell photons. The above WI are a consequence of the gauge invariance of the amplitude in Equation (31) under gauge transformations of the theory that in the momentum space read : $\epsilon^{\mu}(k) \to \epsilon^{\mu}(k) + k^{\mu}$, $\epsilon^{\alpha\beta}(q) \to \epsilon^{\alpha\beta}(q) + q^{\alpha}\varepsilon^{\beta} + q^{\beta}\varepsilon^{\alpha} - 1/2 g^{\alpha\beta}q\cdot\varepsilon$ (with ε a generic four-vector).

Finally, by summing over photon and spin-two polarizations and integrating over the final phase space (see [103,104] for the expression of the polarization matrix of a massive spin-two field), the total width for the $H \to \gamma G$ decay is given by

$$\Gamma(H \to \gamma G) = \frac{F_G^2 m_H^3 m_G^2}{16\pi}(1 - r_G)^3, \tag{34}$$

where $r_G = m_G^2/m_H^2$. As we can see from these results, the above width vanishes in the $m_G \to 0$ limit, as expected from angular momentum conservation.

We stress that the amplitude in Equations (31) and (32) cannot arise at tree level and is expected to be induced only by higher-order contributions in perturbation theory. In particular, since $H \to \gamma G$ is a C-parity violating process, one can easily check that, due to the C-parity conservation of electromagnetic interactions, its contribution exactly vanishes at one loop in the SM and beyond. Then, a (finite) non-vanishing contribution to the F_G form factor can only arise starting from the next-to-leading order at two loops, due to potential corrections induced by C-parity violating interactions [Notice that, thanks to the WI in Equation (33), the corresponding UV contribution is finite at any order in perturbation theory within the SM and in any of its NP extensions, provided the spin-two field acts only

as an external classical source without propagating in the loops]. The computation of this effect at two loops in the SM goes beyond the purpose of the present review.

We will now show that BR$(H \to \gamma G)$ is in general expected to be too small to be observable. From dimensional grounds, one can see that the loop induced F_G form factor should be proportional to $\sim \alpha/\Lambda_G^2$ with Λ_G defined in Equation (29) (neglecting both the loop suppression factors at denominator and other coupling products) which implies that the total width $\Gamma(H \to \gamma\, G)$ is proportional to $\sim \alpha\, m_H^3 m_G^2/\Lambda_G^4$. As shown in [105], the Λ_G effective scale is expected to be not smaller than $(1-100)$ TeV (depending on the value of the graviton mass) for light invisible spin-two fields with masses between the eV and the GeV scale and even heavier for larger masses (for more details see [105]). For $m_G \lesssim 100$ MeV, the corresponding BR would be too small to be observed even for $\Lambda_G \sim 1$ TeV, hence strongly disfavouring any massive spin-two explanation for the $H \to \gamma X$ signal.

Finally, the above arguments could be extended —cum granus salis—to show that also BR$(H \to \gamma X_S)$, with X_S a dark boson with spin $S > 2$, is expected to be strongly suppressed. Although, there is not any consistent S-matrix theory for interacting higher spin fields with $S > 2$, we can estimate the corresponding BR using angular momentum conservation. The argument is the following. For massless X_S particles with spin $S > 1$ in $D = 4$ dimensions, only the two $h = \pm S$ helicity states are available [This result follows from the number of helicity states n_h for a massless particle of spin S in D dimensions, given by $n_h = (D + 2S - 4)(S + D - 5)!/(S!(D-4)!)$ that for $D = 4$ is always $n_h = 2$ [106]]. Then, as for the massless spin-two case discussed above, the Higgs boson cannot decay into a photon plus a massless $X_{S>1}$ boson due to angular momentum conservation. Therefore, it is expected that also in this case, for massive higher spin particles, the decay can only proceed via its $S_z = \pm 1$ spin components. However, the corresponding $S_z = \pm 1$ contributions to the amplitude should vanish in the $m_G \to 0$ limit in order to reproduce the massless limit. Therefore, also for $S > 2$, we expect the width to be strongly suppressed by terms of order m_S^2/m_H^2, thus recovering the same conclusions as for a light spin-two X boson state.

Apart from the two-body decays just discussed, there is the possibility that the two-body signature might be faked by three-body final states with one photon plus missing energy. In particular, three-body final states with two invisible particles, one of which is very soft, can show up with an almost resonant monochromatic photon, with energy $\sim m_H/2$ in the Higgs rest frame, plus missing energy. This case has been considered for instance in [107] in the framework of SUSY models. In this context, the final state is generated in two steps. First, the Higgs boson decays into a neutralino (N) plus a light (invisible) gravitino ($\tilde{g}$), $H \to N\tilde{g}$. Then the neutralino decays into a photon plus gravitino, $N \to \tilde{g}\gamma$, with the two gravitinos giving missing energy in the detector. This signature can fake the dark photon one only if the neutralino is not much lighter than the Higgs boson, so that one of the gravitinos is very soft and goes undetected. However, as shown in [107], the LHC can almost rule out this possibility at the 95% CL, depending on the integrated luminosity and branching ratios of SUSY decays.

In conclusion, a monochromatic photon signature in the Higgs $H \to \gamma X$ decay would in practice uniquely identify the X particle as a dark photon.

3. Dark Photon Production in Higgs Decays at LHC

In this section, we summarize the main results of our phenomenological studies [91,92] of the dark photon production via Higgs decay at the Large Hadron Collider experiment at CERN. LHC is the world's largest particle accelerator to date where *proton–proton* collisions take place at high center-of-mass (c.m.) energies. The main Higgs production channels in proton–proton collisions are the Higgs production via gluon fusion (ggF), VBF and associated production (VH).

3.1. Gluon Fusion Production

Higgs production via a gluon fusion process is one of the dominant modes at the LHC. The estimated cross section in this channel is 49.85 (19.37) pb at 14 (8) TeV c.m.

energy, and gives the largest production rate for a hypothetical scalar boson with SM Higgs-like couplings for the entire mass range of interest [108]. We have simulated the $pp \to H \to \gamma\gamma_D$ process, where the Higgs is produced in the gluon fusion channel both at 8 TeV and 14 TeV c.m. energies. The Feynman diagram for this process is depicted in Figure 4 (left). The signal is characterized by *a single photon recoiling against missing transverse momentum* $(\gamma + \not{E}_T)$. The SM backgrounds for this process are dominated by $pp \to \gamma j$ and QCD multi-jet background $pp \to$ jets, where the missing transverse momentum can arise from a number of sources, e.g., (a) jet energy mismeasurement, (b) invisible neutrinos arising from decays of heavy-flavor jets, and (c) very forward particles escaping the detector. The latter process contributes to the $\gamma + \not{E}_T$ final state whenever one of the jets is misidentified as a photon. The main electroweak background consists of the channels $pp \to W \to e\nu$, where the electron is misidentified as a photon, $pp \to W(\to \ell\nu)\gamma$, for ℓ outside charged-lepton acceptance, and $pp \to Z(\to \nu\nu)\gamma$.

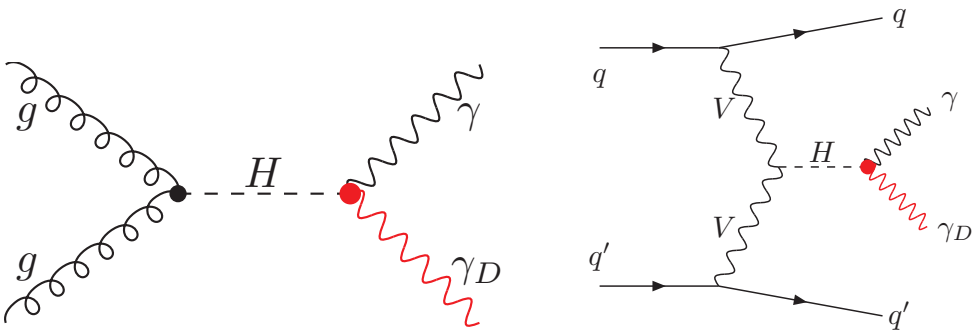

Figure 4. Feynman diagrams for the Higgs production via gluon fusion (**left**), and VBF (**right**) channels at the LHC.

We have simulated both the parton level signal and background events in the context of the gluon fusion process using ALPGEN (v2.14) event generator [109]. The signal processes generated by ALPGEN consist of $pp \to H$ and $pp \to Hj$, whereas those for the backgrounds are $pp \to \gamma j$ and $pp \to jj$. The other electroweak backgrounds such as $pp \to W$, $pp \to W\gamma$, and $pp \to Z\gamma$, are generated using Mad-Graph5 aMC@NLO (v2.2.2) [110]. These events are then interfaced with PYTHIA (v6.4) [111] for parton shower, hadronization, and clustering of these hadrons to obtain jets using a simple cone algorithm. More importantly, the decay of the Higgs into a photon and dark photon has also been ensured at the PYTHIA level using appropriate branching fraction. We have also implemented a finite detector resolution effect on the final state reconstructed objects assuming a Gaussian smearing function.

Several kinematic observables, such as missing transverse energy ($\not{E}_T$), transverse momentum of the photon (p_T^γ), and transverse mass of the photon-invisible system ($M^T_{\gamma\gamma_D}$) have been proposed to isolate the signal from the SM backgrounds [91,92]. The transverse mass variable that carries the typical signature of the $H \to \gamma\gamma_D$ decay is defined as $M^T_{\gamma\gamma_D} = \sqrt{2p_T^\gamma \not{E}_T(1 - \cos\Delta\phi)}$, where $\Delta\phi$ is the azimuthal distance between the photon transverse momentum p_T^γ and the missing transverse momentum $\not{E}_T$. The $\not{E}_T$ is defined as the unbalanced momentum in the transverse plane due to the presence of the invisible particles. Figure 5 (left plot) depicts the expected distribution of the $M^T_{\gamma\gamma_D}$ variable for the signal and SM backgrounds in the gluon fusion channel.

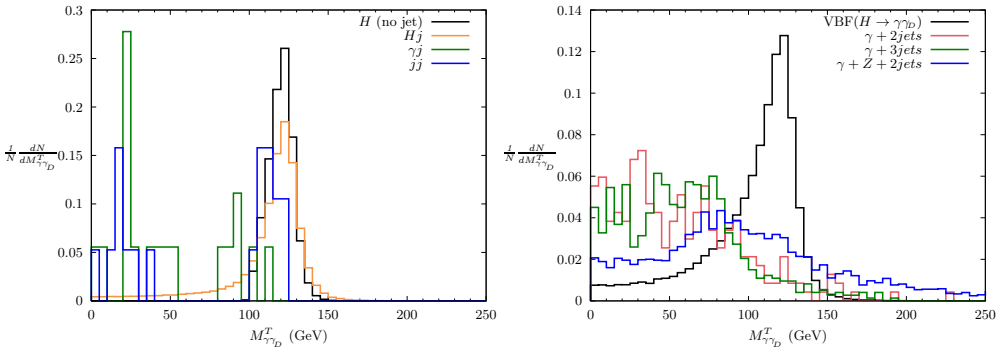

Figure 5. Transverse-mass distributions for the $H \to \gamma\gamma_D$ signal in the gluon fusion process (**left**), and VBF process (**right**) [92]. Corresponding distributions for SM backgrounds for inclusive $\gamma + \not{E}_T$ (ggF) and $\gamma + \not{E}_T +$ two forward jets (VBF) final states (with no isolated leptons), respectively, have also been shown. All distributions are normalized to unity.

The results of our simulation are summarized in Table 2 in terms of the cross section times cut efficiency ($\sigma \times A$) of the signal and the background processes after the implementation of the event selection criteria detailed in [92] at two different c.m. energies, 8 TeV and 14 TeV, assuming BR($H \to \gamma\gamma_D$) $\sim$ 1%. Due to large QCD backgrounds and poor estimates of the missing transverse momentum arising from jet energy mismeasurement, one has less control over the SM background in this channel. Using as significance estimator $S/\sqrt{S+B}$, the analysis at 8 TeV with the 20 fb^{-1} data set gives a 5σ discovery reach at $\mathrm{BR}_{\gamma\gamma_D} \simeq 4.8 \times 10^{-3}$.

In Table 3, we present the 2σ exclusion limit and the 5σ discovery potential for $\mathrm{BR}_{\gamma\gamma_D}$ after extrapolating the optimization technique to 14 TeV center of mass energy at three different integrated luminosities. At an integrated luminosity of 100 (300)fb^{-1} the 2σ exclusion limit on $\mathrm{BR}_{\gamma\gamma_D}$ is found to be $6.4 \times 10^{-4}(3.7 \times 10^{-4})$, whereas the 5σ discovery reach is $1.6 \times 10^{-3}(9.2 \times 10^{-4})$. The corresponding 5σ reach can be improved down to 2.9×10^{-4} at the High-Luminosity LHC (HL–LHC), with an integrated luminosity of 3 ab^{-1} [92].

Table 2. Cross section times acceptance A (in fb) for the gluon fusion signal and corresponding SM backgrounds at 8 and 14 TeV, assuming $\mathrm{BR}_{\gamma\gamma_D}$ = 1%, with the selection $p_T^\gamma > 50$ GeV, $|\eta^\gamma| < 1.44$, $\not{E}_T > 50$ GeV, and 100 GeV $< M^T_{\gamma\gamma_D} <$ 130 GeV [92].

	$\sigma \times A$ [8 TeV]	$\sigma \times A$ [14 TeV]
$H \to \gamma\gamma_D$ ($\mathrm{BR}_{\gamma\gamma_D} = 1\%$)	**44**	**101**
γj	63	202
$jj \to \gamma j$	59	432
$e \to \gamma$	55	93
$W(\to \ell\nu)\gamma$	58	123
$Z(\to \nu\nu)\gamma$	102	174
total background	337	1024

Table 3. Reach in $\mathrm{BR}_{\gamma\gamma_D}$ (in percentage) for a 95% C.L. (2σ) exclusion or a 5σ discovery at the 14 TeV LHC, in the VBF and gluon fusion channels, for different integrated luminosities L [92,112].

$\mathrm{BR}_{\gamma\gamma_D}$ (%)	L = 100 fb^{-1}		L = 300 fb^{-1}		L = 3 ab^{-1}	
Significance	2σ	5σ	2σ	5σ	2σ	5σ
$\mathrm{BR}_{\gamma\gamma_D}$(VBF)	0.76	1.9	0.43	1.1	0.14	0.34
$\mathrm{BR}_{\gamma\gamma_D}$ (ggF)	0.064	0.16	0.037	0.092	0.012	0.029

3.2. Vector Boson Fusion (VBF) Production

Here we discuss the phenomenological study of the Higgs production in the VBF process and its subsequent decay to $H \to \gamma\gamma_D$. The VBF production channel is the most dominant mode of Higgs production at the LHC after ggF, with an estimated cross section of 4.18 (1.578) pb at 14 (8) TeV c.m. energy [108]. The final state in this case ($pp \to Hjj \to \gamma\gamma_D jj$) consists of an isolated photon, missing transverse energy and two forward jets with opposite rapidity. The corresponding Feynman diagram is shown in Figure 4 (right). The SM background contributions to this final state mainly come from γ+jets, QCD multi-jets, and $\gamma + Z(\to \bar{\nu}\nu)$+jets processes. Given the magnitude of QCD multi-jets background, even a jet faking as a photon with a mistagging rate of 0.1% gives a dominant background contribution to our final state as discussed in the ggF study. The identification efficiency of a true photon is assumed to be the same as that is used in the ggF process.

In this case, the parton level signal events for $pp \to Hjj$ via the VBF channel are generated using a Madgraph event generator, whereas the parton level background events for the processes $pp \to \gamma + jets$, QCD multijets, and $pp \to \gamma + Z + jets$ are all generated using an ALPGEN event generator. The remaining steps such as parton showering, hadronization, decay, and clustering of hadrons into jets are all performed using PYTHIA. The energy momenta of the final state reconstructed objects have been smeared in a similar manner.

The results of our phenomenological analysis is presented in Table 4 which contains the cross sections times cut acceptance for the signal and dominant SM backgrounds after the sequential application of basic cuts, rapidity cuts on the two forward jets, and transverse mass cut on the photon plus missing transverse energy system as described earlier. In this case, the missing transverse mass variable ($M^T_{\gamma\gamma_D}$) [see Figure 5 (right plot)] alsoturns out to be particularly useful to suppress the SM backgrounds. Assuming an integrated luminosity of 100 fb^{-1}, the 5σ reach in the branching ratio is about BR$_{\gamma\gamma_D} \simeq 2\%$. With the HL–LHC integrated luminosity of 3 ab^{-1}, the 5σ reach can be extended down to BR$_{\gamma\gamma_D} = 3.4 \times 10^{-3}$. A comparison of significances for both of these Higgs production channels is presented in Table 3 [92,112].

Table 4. Cross section times acceptance $\sigma \times A$ (in fb) for the VBF signal and backgrounds at 14 TeV, after sequential application of cuts defined in the text, assuming) BR$_{\gamma\gamma_D}$ = 1% [92].

Cuts	Signal	γ + Jets	γ + Z + Jets	QCD Multiijet
Basic cuts	17.7	266,636	1211	72,219
Rapidity cuts	8.8	8130	38.1	33,022
$M^T_{\gamma\gamma_D}$ cuts	5.0	574	6.5	3236

4. Experimental Searches at the LHC

In this section, we summarize present experimental LHC results on dark photon production via Higgs decay in two different Higgs production channels, namely, VBF and Higgs production in association with a Z-boson (ZH).

4.1. VBF Production

Both the ATLAS and CMS experiments studied the $pp \to \gamma + \not{E}_T + jets$ via Higgs production in VBF channel [93,94]. The data collected in this channel has been interpreted in the context of Higgs production through VBF and its subsequent decay to a photon and massless dark photon which goes undetected, $pp \to Hjj \to \gamma\gamma_D jj$.

The SM backgrounds for this process are $V\gamma + jets$, where $V = Z, W$ and $\gamma + jets$. In case of $Z\gamma + jets$, the Z decays to a pair of $\nu\bar{\nu}$ and gives rise to isolated photon, missing transverse momentum, and jets. $W\gamma + jets$ contribute to the same final state when the $W^{\pm}$ boson decays to a lepton and a neutrino, and the lepton goes missing as it may not satisfy the required identification criteria. One can also have a contribution from $W\gamma + jets$ and $W\gamma + jets$ process with a jet being mistagged as a photon.

4.1.1. ATLAS

The ATLAS experiment at the LHC is a particle detector having a cylindrical geometry with forward–backward symmetry. It consists of mainly four parts: the inner-most tracking detector, electromagnetic and hadronic calorimeter (ECAL and HCAL), and the outer muon spectrometer. The tracking detector which is used to measure the momentum of charged particles has a rapidity coverage of $|\eta| < 2.5$. The ECAL and HCAL coverage is up to $|\eta| < 4.9$. The inner tracking detector is provided with a 2.0 T axial magnetic field produced by a surrounding superconducting solenoid. The muon spectrometer is based on large superconducting toroidal magnets and provides an integral field in the range 2.0 T to 6.0 T.

The ATLAS analysis of $H \to \gamma\gamma_D$ in the VBF channel corresponds to 139 fb^{-1} data collected by the ATLAS collaboration during 2015–2018 at 13 TeV LHC collision energy [93]. An ATLAS experiment uses several kinematic variables similar to those discussed in Section 3.2 in addition to their dedicated object reconstruction criteria.

The results of ATLAS analysis can be used to set limits on the cross section of Higgs production in the VBF channel times BR($H \to \gamma\gamma_D$) as a function of the hypothetical neutral Higgs boson in the mass range 60 GeV $< m_H <$ 2 TeV (Figure 6). The corresponding bound obtained by the ATLAS experiment is 0.19 pb. Assuming an SM-like Higgs production cross section in the VBF channel in this mass range, the results can be interpreted as a bound on BR($H \to \gamma\gamma_D$). For the SM Higgs boson ($m_H \simeq 125$ GeV), the 95% C.L. upper bound on BR($H \to \gamma\gamma_D$) obtained by the ATLAS collaboration corresponds to 0.014.

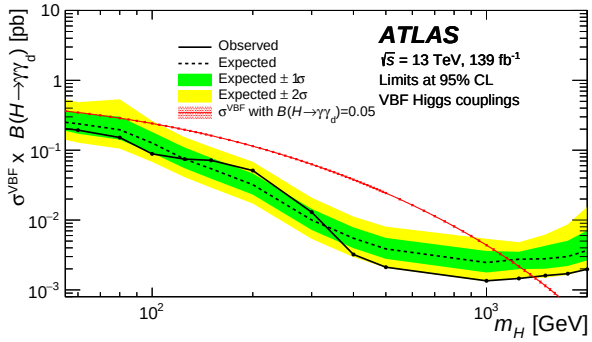

Figure 6. Observed and expected 95% C.L. upper limit on the Higgs production cross section times BR($H \to \gamma\gamma_D$), for various scalar mass hypothesis [93]. The red line corresponds to the theoretical SM-like Higgs production cross section in VBF channel times BR($H \to \gamma\gamma_D$)$\sim$ 5%.

4.1.2. CMS

The CMS detector also consists of an inner tracker, electromagnetic calorimeter, hadronic calorimeter, and muon detector. The inner tracker operates in the range $|\eta| < 2.5$. The ECAL and HCAL has rapidity coverage of $|\eta| < 3.0$. In addition, the forward calorimeter provides a rapidity coverage up to $|\eta| < 5.0$. CMS also has a dedicated muon detector which constitute the outer most layer of the CMS detector.

The results of the corresponding CMS analysis in the VBF channel are shown in Figure 7 which correspond to 130 fb^{-1} of data collected by CMS collaboration during 2016–2018 at 13 TeV LHC collision energy [94]. The observed 95% C.L. on the $H \to \gamma\gamma_D$ branching ratio obtained by CMS collaboration in the VBF channel is 3.5% for the SM Higgs boson with $m_H = 125$ GeV [94].

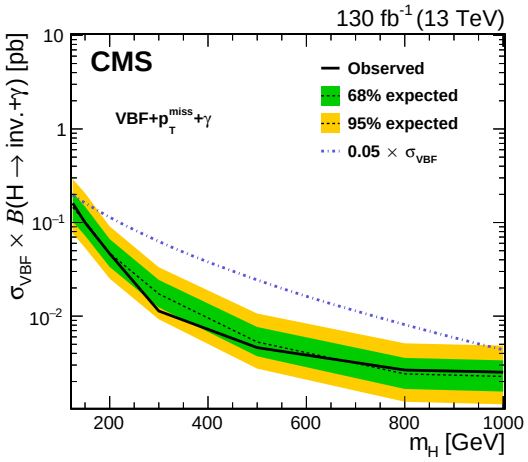

Figure 7. CMS bound on the cross section (σ_{VBF}) times BR($H \to$ inv. $+ \gamma$) in the VBF channel as a function of the scalar mass (m_H) [94]. Solid black line corresponds to the observed limit, while the black dashed line corresponds to the expected limit at 95% C.L. The dotted dashed line represents the signal corresponding to a SM σ_{VBF} value and BR($H \to$ inv. $+ \gamma$) = 5%.

4.2. ZH Production

CMS

The CMS collaboration has also studied the Higgs production in association with a Z-boson in pp collisions with subsequent decay of the Higgs into a photon plus an undetected particle using the 137 fb^{-1} of data collected at 13-TeV pp c.m. energy [95]. In the absence of any significant excess over the SM backgrounds an exclusion limit can be set on theoretical models predicting such exotic decay of the Higgs boson. The results of CMS study has been interpreted in the context of models predicting $H \to \gamma\gamma_D$ decay and the corresponding process $pp \to ZH \to (Z \to \ell^-\ell^+)(H \to \gamma\gamma_D)$. The Feynman diagram for the above process is shown in Figure 8.

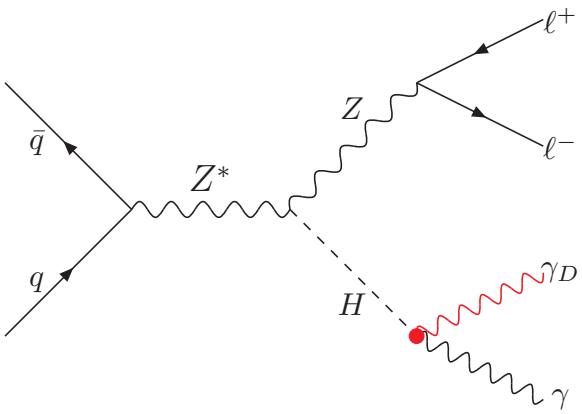

Figure 8. Feynman diagrams for the Higgs production in association with the Z-boson and the subsequent decay $H \to \gamma\gamma_D$ at the LHC. The red bubble stands for the effective $H\gamma\gamma_D$ vertex.

The main backgrounds to the final state under consideration as analyzed by CMS are ZW, ZZ, and $Z\gamma$. For ZW and ZZ, the contribution comes when a lepton is misidentified as a photon.

The results of the CMS analysis in the ZH channel are presented in Figure 9, which provides an exclusion limit on the cross section times branching ratio of the Higgs in the *photon+invisible* mode [95]. If the data is interpreted in the context of theoretical models predicting a $H \to \gamma\gamma_D$ decay, a bound on cross section times BR($H \to \gamma\gamma_D$) $\sim$ 0.04 pb can

be obtained for $m_H \simeq 125$ GeV. The observed 95% C.L. upper bound on BR($H \to \gamma\gamma_D$) obtained by CMS is 4.6% for the SM Higgs boson with $m_H \simeq 125$ GeV.

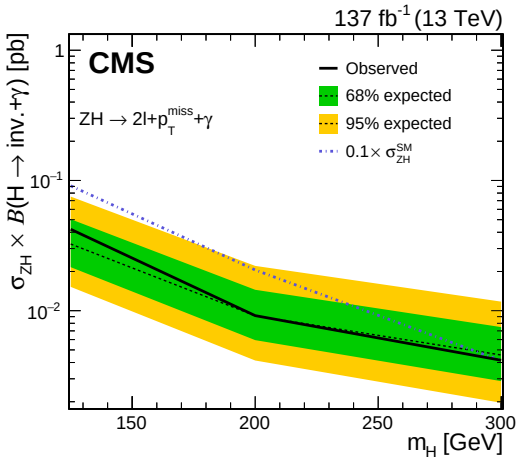

Figure 9. CMS bound on the cross section (σ_{ZH}) times BR($H \to$ inv. $+ \gamma$) in the ZH channel as a function of the scalar mass (m_H) [95]. Solid black line corresponds to the observed limit while the black dashed line corresponds to the expected limit, at 95% C.L.. The dotted dashed line represents the signal corresponding to a SM σ_{ZH} value and BR($H \to$ inv. $+ \gamma$) $= 10\%$.

The CMS collaboration also extended the analysis for a heavier hypothetical neutral scalar boson in the mass range 125 GeV to 300 GeV with similar decay mode.

The CMS bound from ZH, VBF, and combined analysis are summarized in Table 5, for the SM Higgs boson with $m_H \simeq 125$ GeV.

Table 5. Observed and expected 95% C.L. upper limits on BR($H \to$ inv. $+ \gamma$) at $m_H \simeq 125$ GeV, from the VBF, ZH channels, and the combined analysis [94].

VBF		***ZH***		**VBF + *ZH***	
Obs. (%)	**Exp. (%)**	**Obs. (%)**	**Exp. (%)**	**Obs. (%)**	**Exp. (%)**
3.5	$2.8^{+1.3}_{-0.8}$	4.6	$3.6^{+2.0}_{-1.2}$	2.9	$2.1^{+1.0}_{-0.7}$

4.3. Future Perspectives at the LHC

The future prospects of dark photon searches at the HL–LHC via Higgs production in pp collisions are summarized in Table 6 [including also the possibility of a High Energy (HE) LHC at $\sqrt{s} = 27$ TeV]. Using a similar analysis as that implemented by CMS at $\sqrt{S} = 8$ TeV which can provide a good control over the overwhelming $\gamma + jets$ and jj backgrounds (called "CMS inspired" in Table 6), one can achieve the strongest limit on BR($H \to \gamma\gamma_D$). At a c.m. energy 14 (27) TeV with integrated luminosity of 3 (15) ab^{-1}, the expected 5σ discovery reach on the BR($H \to \gamma\gamma_D$) is $\sim 3 \times 10^{-4}$ (1.3×10^{-4}), while the corresponding expected 2σ exclusion limit on the Higgs branching ratio in the same mode is found to be $\sim 1.2 \times 10^{-4}$ (0.5×10^{-4}) [113].

Table 6. The future projection at the HL–LHC and HE–LHC in terms of discovery (5σ) reach and exclusion (2σ) limit for BR($H \to \gamma\gamma_D$) (in %) [112,113].

BR$_{\gamma\gamma_D}$ (%)	**3 ab^{-1}@14 TeV**		**15 ab^{-1}@27 TeV**	
significance	2σ	5σ	2σ	5σ
CMS inspired	0.012	0.030	0.0052	0.013

5. Dark Photon Production at Future e^+e^- Colliders

It is also important to look at future prospects for dark photon searches via Higgs production in the context of various proposed future e^+e^- colliders. In [96], we have shown that one could improve the sensitivity to the $H \to \gamma\gamma_D$ branching ratio at future e^+e^- collider experiments. In particular, the proposed Future Circular e^+e^- Collider (FCCee) is deemed to run with high luminosity at c.m. energies $[91.2, 161, 240, 350(365)]$ GeV, corresponding, respectively, to the Z pole and to the approximate WW, ZH and $t\bar{t}$ thresholds [114]. We have proposed both direct dark photon production in association with a Higgs boson ($e^+e^- \to H\gamma_D$) [96], and the dark photon production in the decay of a Higgs boson [$e^+e^- \to ZH \to Z(H \to \gamma\gamma_D)$] [97], by focusing on the c.m. energy $\sqrt{s} \simeq 240$ GeV with integrated luminosity of 10 ab^{-1}.

In the context of e^+e^- colliders, all the signal and background events are generated using a Madgraph event generator and then interfaced with PYTHIA for further analysis. However, to simulate the process $e^+e^- \to H\gamma_D$ using Madgraph we have to implement the appropriate effective operators $(F^{\mu\nu}F^D_{\mu\nu}H)$, $(Z^{\mu\nu}F^D_{\mu\nu}H)$ in the Madgraph model file. This has been accomplished with the help of FeynRules (v2.0) [115], where we have implemented these operators at the Lagrangian level, and the corresponding output of the FeynRules are then interfaced with Madgraph.

- The study of $e^+e^- \to H\gamma_D \to (H \to b\bar{b})\gamma_D$ illustrates a novel signature in which an invisible massless system recoils against a $b\bar{b}$ system with invariant mass close to the Higgs mass. This is a unique feature of a massless dark photon produced in association with a Higgs. The corresponding Feynman diagram is shown in Figure 10. Due to the clean environment in a e^+e^- collider and definite knowledge of the initial state, one can in principle reconstruct the full four-momentum of the invisible dark photon system. The SM backgrounds to the $b\bar{b} + missing\ energy$ final states are $\nu\bar{\nu}b\bar{b}$ and $\nu\bar{\nu}q\bar{q}$. The contribution to the missing energy ($\not{E}$) in the background process is due to the pair of invisible almost massless neutrinos. Here, missing energy is defined as $\not{E} = \sqrt{s} - \sum \mathrm{E}_{visible}$ where the sum is over all the visible particles. In [96], we have pointed out how introducing various kinematic variables such as invariant mass of the two leading jets (M_{jj}), missing energy ($\not{E}$), and missing mass ($M_{\rm miss}$) one can efficiently suppress the SM background. The variable missing mass is defined as $M_{\rm miss} = \sqrt{\not{E}^2 - \not{\mathbf{p}}^2}$ where $\not{\mathbf{p}} = -\sum \mathbf{p}_{visible}$ is the final-state missing a three-momentum vector. The missing mass plays a crucial role to separate the signal from SM backgrounds. For the signal process, the corresponding distribution is centered around $M_{\rm miss} = 0$ due to the presence of a single massless dark photon in the final state [see Figure 11 (left)].
  In Table 7, we summarize the cross sections and cut efficiencies for the signal and background processes. For detailed event selection criteria see [96]. The corresponding sensitivity reach as a function of $C_{\gamma\gamma_D}$ and $C_{Z\gamma_D}$ is shown in Figure 12, which illustrates that, at 95% C.L., one can exclude $C_{\gamma\gamma_D} > 1.9$ (for $C_{Z\gamma_D} = 0$). This can be translated to an exclusion limit on the BR($H \to \gamma\gamma_D$) greater than three times the SM BR($H \to \gamma\gamma$). For $C_{\gamma\gamma_D} = 0$, the corresponding exclusion limit is $C_{Z\gamma_D} > 2.7$, and for $C_{Z\gamma_D} \simeq 0.79\ C_{\gamma\gamma_D}$ the exclusion limit is $C_{\gamma\gamma_D} > 1.6$.

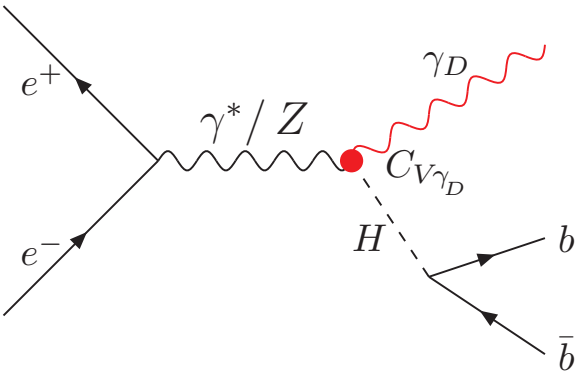

Figure 10. Feynman diagrams for the $H\gamma_D$ production at e^+e^- colliders. The red bubble stands for the effective Higgs $HV\gamma_D$ vertex, with $V = \gamma^*/Z$.

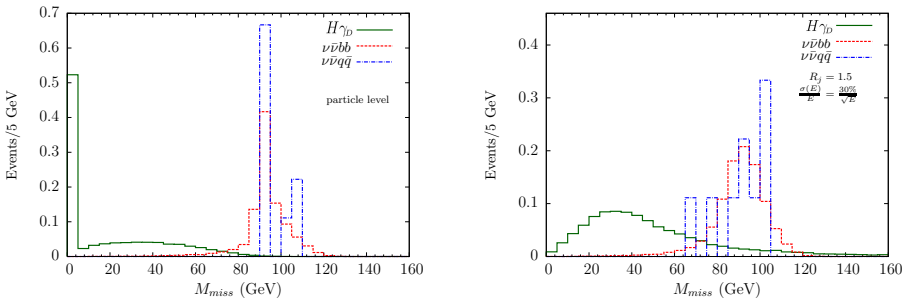

Figure 11. Missing mass distribution without (***left***) and with (***right***) taking into account the effects of finite detector resolution in the $e^+e^- \to H\gamma_D \to (H \to b\bar{b})\gamma_D$ channel [96].

Table 7. Cross sections (in fb) and corresponding acceptances after kinematical cuts on signal and SM backgrounds at $\sqrt{s}$ =240 GeV [96]. Applied cuts include basic cuts for object reconstruction, dijet invariant mass (M_{jj}) to be within 10% of the M_{jj} peak value of signal events, $M_{\text{miss}} < 40$ GeV, and $\not{E} < 100$ GeV. Cross sections include BR$(H \to b\bar{b}) \simeq 0.58$.

Process	**Cross Section (fb)**	**Acceptance after Cuts (%)**
$H\gamma_D \quad (C_{Z\gamma_D} = 0)$	$10.1 \times 10^{-3}\ C^2_{\gamma\gamma_D}$	17.3
$H\gamma_D \quad (C_{\gamma\gamma_D} = 0)$	$4.8 \times 10^{-3}\ C^2_{Z\gamma_D}$	17.3
$H\gamma_D \quad (C_{Z\gamma_D} = 0.79\ C_{\gamma\gamma_D})$	$13.8 \times 10^{-3}\ C^2_{\gamma\gamma_D}$	17.3
SM $\nu\bar{\nu}b\bar{b}$	115.	0.08

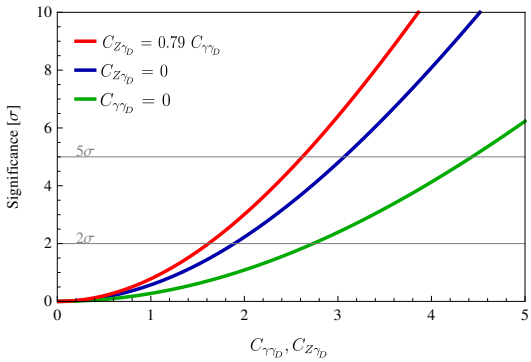

Figure 12. Estimated signal significance ($S/\sqrt{S+B}$) as a function of the effective couplings $C_{\gamma\gamma_D}, C_{Z\gamma_D}$ for $e^+e^- \to H\gamma_D$ channel at a center of mass energy 240 GeV and integrated luminosity of 10 ab^{-1} [96]. olid green line represents the signal significance for $C_{\gamma\gamma_D} = 0$, solid blue line represents the same for $C_{Z\gamma_D} = 0$, while the solid red line corresponds the to the case $C_{Z\gamma_D} = 0.79 C_{\gamma\gamma_D}$. The 5σ discovery reach and 2σ exclusion limit are shown by the upper and lower horizontal gray lines, respectively.

- The dark photon production via Higgs decay at the future e^+e^- collider, $e^+e^- \to ZH \to Z(H \to \gamma\gamma_D)$ provides a better sensitivity to the $H \to \gamma\gamma_D$ branching ratio. We have proposed two different final states considering both leptonic and hadronic decay modes of the Z-boson. The leptonic final state in $e^+e^- \to ZH \to (Z \to \mu^-\mu^+)(H \to \gamma\gamma_D)$ consists of a pair of opposite sign muons, an isolated photon and missing energy due to the presence of a massless invisible dark photon. In the hadronic final states, the muon pair is replaced by a pair of jets in $e^+e^- \to ZH \to (Z \to q\bar{q})(H \to \gamma\gamma_D)$. The corresponding SM background contributions dominantly come from $e^+e^- \to ZH \to Z(H \to \gamma\gamma)$ and $e^+e^- \to Z\gamma\gamma$ when one of the photons is not detected at the detector and/or lies in the forward region. The Feynman diagram(s) for this process is illustrated in Figure 13. The kinematic variables, such as missing energy ($\not{E}$) and missing mass (M_{miss}) proposed in the previous analysis along with dimuon/dijet invariant mass variable ($M_{\mu^+\mu^-/jj}$), help to reduce the contribution of these SM backgrounds. In addition, one has the advantage of using invariant mass of the *photon+dark photon system* ($M_{\gamma\gamma_D}$) to further discriminate the signal from backgrounds, thanks to the full reconstruction of the dark photon momenta in an e^+e^--colliding environment. For the signal process, the last three kinematic distributions are centered around $M_{\text{miss}} = 0$, $M_{\mu^+\mu^-/jj} = M_Z$, and $M_{\gamma\gamma_D} = m_H$, respectively. In Tables 8 and 9 , we summarize the cut-flow effects for both the dimuon and dijet ($+\gamma + \not{E}$) final states after imposing a set of event selection criteria detailed in [97].

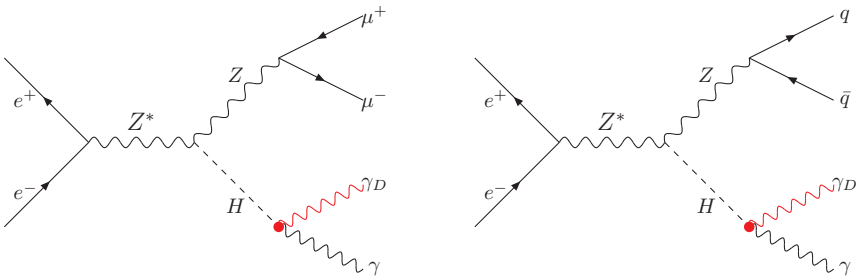

Figure 13. Feynman diagrams for dark photon production in e^+e^- collisions via associated ZH production. The red bubble stands for the effective $H\gamma\gamma_D$ vertex.

Table 8. Event yields after sequential cuts for $e^+e^- \to ZH \to \mu^+\mu^-\gamma\gamma_D$ and corresponding background, for an integrated luminosity of 10 ab^{-1}, and c.m. energy $\sqrt{s} = 240$ GeV [97]. The signal yield has been normalised assuming BR($H \to \gamma\gamma_D$)= 0.1%.

Process	Basic Cuts	$M_{\ell\ell}$ Cut	$M_{\gamma\gamma_D}$ Cut	M_{miss} Cut
$\mu^+\mu^-\gamma\gamma_D$ (BR$_{\gamma\gamma_D} = 0.1\%$)	65.3	54.9	49.7	47.3
$\mu^+\mu^-\nu\bar{\nu}\gamma$	5.00×10^4	5.73×10^3	1.09×10^3	15

Table 9. Event yields for $e^+e^- \to ZH \to q\bar{q}\gamma\gamma_D$, after sequential cuts discussed in [97], and corresponding backgrounds rates, for an integrated luminosity of 10 ab^{-1}, and c.m. energy $\sqrt{s} = 240$ GeV. The signal yield has been normalised assuming BR($H \to \gamma\gamma_D$)= 0.1%. Dashes stand for event yields less than 1.

Process	Basic Cuts	M_{jj} Cut	$M_{\gamma\gamma_D}$ Cut	M_{miss} Cut	$\not{E}$ Cut
$jj\gamma\gamma_D$ (BR$_{\gamma\gamma_D} = 0.1\%$)	804	669	154	110	72
$jj\gamma$	3.39×10^7	2.26×10^7	1.47×10^5	6.5×10^4	–
$jj\nu\bar{\nu}\gamma$	3.9×10^4	3.1×10^4	5.9×10^3	2.2	–

The sensitivity reach as a function of BR($H \to \gamma\gamma_D$) is depicted in Figure 14 for an integrated luminosity of 10 ab^{-1} at $\sqrt{s} = 240$ GeV. Clearly, the hadronic channel provides a better discovery reach (or exclusion limit) compared to the dimuon channel. The combined 5σ sensitivity for discovery reaches BR($H \to \gamma\gamma_D$) $\simeq 2.7 \times 10^{-4}$, while the 95% C.L. exclusion limit is again BR($H \to \gamma\gamma_D$) $\simeq 0.5 \times 10^{-4}$.

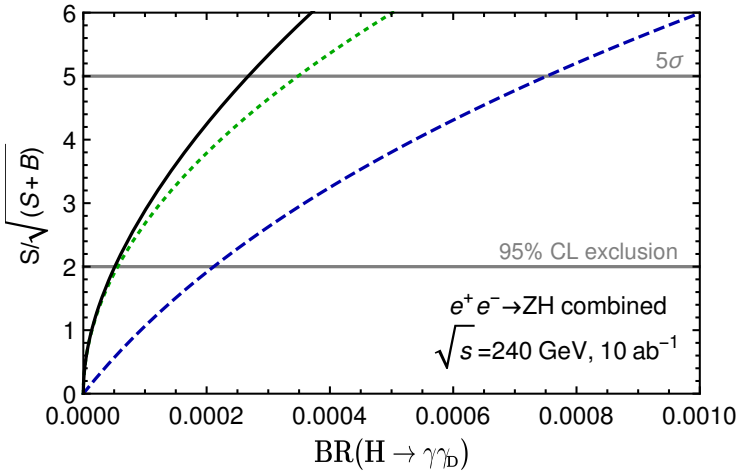

Figure 14. Estimated signal significances vs the branching ratio of $H \to \gamma\gamma_D$ for $e^+e^- \to ZH$ channel at a center of mass energy 240 GeV and integrated luminosity of 10 ab^{-1} [97]. The blue dashed line corresponds to the estimated significance in the dimuon+$\gamma + \not{E}$ final state, the green dotted line corresponds to that in the dijet+$\gamma + \not{E}$ final state, while the significance in the combined channel is represented by the solid black line. The 5σ discovery reach and 2σ exclusion limit are shown by the upper and lower horizontal gray lines, respectively.

6. Conclusions

We have explored Higgs-mediated dark photon production at the LHC and future colliders via the Higgs decay into a photon and a dark photon $H \to \gamma\gamma_D$. We have assumed the dark photon to be massless and associated to an unbroken $U(1)_D$ gauge symmetry in the dark sector. Contrary to the massive case, a massless dark photon is only coupled to the SM fields via higher dimensional operators, which are suppressed by the unknown UV scale Λ. Then, depending on Λ, dark photon direct production at colliders is in general

strongly suppressed by terms of order $\mathcal{O}(E/\Lambda)^2$, with E the characteristic energy of the process, thus rendering the search for a massless dark photon dramatically dependent on the UV completion of the theory. Nevertheless, due to its non-decoupling properties, the Higgs boson system contradicts this expectation and offers a privileged strategy to explore the dark photon production by a clean experimental probe.

By using a simplified model with UV completion, we have shown that the $H \to \gamma\gamma_D$ decay might have measurable rates (mostly insensitive to the UV scale) which depend only on a few dimensionless (and potentially large) dark sector parameters. We have assumed the existence of a set of scalar messenger fields connecting the SM and dark sector fields via renormalizable interactions. We have provided correlated predictions for the $H \to \gamma\gamma_D, \gamma_D\gamma_D$ decay rates, and NP exotic contributions to the SM channels $H \to \gamma\gamma, Z\gamma, gg$, from which the non-decoupling properties clearly emerge. Analytical results for the corresponding amplitudes and decay rates are provided in the most general scenario, with generic N scalar messenger fields charged under both SM and $U(1)_D$ gauge interactions.

Since a massless or ultralight γ_D would be experimentally invisible, the typical signature for the $H \to \gamma\gamma_D$ decay at colliders would be characterized by an almost monochromatic photon—with energy half of the Higgs boson mass in its rest frame—plus missing transverse energy. We review the main signatures related to the $H \to \gamma\gamma_D$ decay in the dominant Higgs production channels at the LHC and discuss the most relevant irreducible and reducible backgrounds. In particular, the $H \to \gamma\gamma_D$ decay in the gluon–gluon fusion and VBF mechanisms (analyzed in [91,92]) are discussed and compared with the recent analysis by the ATLAS [93] and CMS [94,95] collaborations for the search of a $H \to \gamma\gamma_D$ signal at the LHC, in VBF and associated-ZH events collected at $\sqrt{s} \simeq 13$ TeV, with about 140fb^{-1}. No significant excess above the SM expectations is found in either experiment, leading to an observed 95% C.L. upper limit on BR$(H \to \gamma\gamma_D)$ of 1.4% (ATLAS) [93] and 2.9% (CMS) [94].

These results are compared with the corresponding predictions for the BR$(H \to \gamma\gamma_D)$ in the UV complete model for the dark sector, where a model-independent parametrization for the $H \to \gamma\gamma_D, \gamma_D\gamma_D$ decay rates has been adopted. In particular, BR$(H \to \gamma\gamma_D)$ regions allowed by all present constraints as a function of the α_D—the fine-structure constant related to the $U(1)_D$ gauge symmetry—have been presented. We have found that the current sensitivity in the BR$(H \to \gamma\gamma_D)$ measurements by ATLAS and CMS, which is at the percent level, is presently one order of magnitude weaker than what is needed for detecting BR$(H \to \gamma\gamma_D)$ in the allowed range, consistent with actual constraints on BR$(H \to \gamma\gamma)$ and BR$(H \to$ invisible$)$. Hence, larger statistics will be needed at the LHC to explore the allowed BR$(H \to \gamma\gamma_D)$ range at the permil level. Future perspectives for the search of the $H \to \gamma\gamma_D$ signal at future e^+e^- colliders and hadron colliders experiments are also shown.

We also discussed possible alternative new physics scenarios that could fake the dark photon signature by analyzing the generic $H \to \gamma X$ decay with X an invisible (light) dark particle. We have shown that the observation of the monochromatic photon signature plus missing energy identifies the dark photon as *by far* the most viable interpretation. Indeed, we have shown that, although both scalar and pseudoscalar X cases are forbidden by angular momentum conservation, bosonic X particles with spin higher than one are in principle possible (while fermionic X states are forbidden by Lorentz invariance). In particular, we have shown that for a massive spin-two field $X = G$ universally coupled to matter fields, the decay rate $H \to \gamma G$ is non-vanishing, but quite suppressed by terms of order m_G^2/Λ^2, with Λ the effective scale associated to the $H\gamma G$ coupling, and m_G the particle mass. The same conclusions also hold for higher spin fields, effectively coupled to the SM fields, whose contribution is also expected to be strongly suppressed by the mass. In conclusion, the potential measurement of the monochromatic photon signature in the $H \to \gamma X$ decay, with X an invisible (light) dark particle X, would in practice uniquely identify X as a dark photon, opening the way to the discovery of this particle as a portal to the dark sector.

All the above features promote the $H \to \gamma\gamma_D$ decay to a golden channel for the dark photon discovery in both massless and massive scenarios.

Author Contributions: All authors have equally contributed to all aspects of the article indicated below. All authors have read and agreed to the published version of the manuscript.

Funding: This research received no external funding.

Institutional Review Board Statement: Not applicable.

Informed Consent Statement: Not applicable.

Data Availability Statement: Not applicable.

Acknowledgments: We thank Damiano Anselmi, Matti Heikinheimo, and Martti Raidal for inspiring discussions.

Conflicts of Interest: The authors declare no conflict of interest.

Reference

1. Aad, G.; Abajyan, T.; Abbott, B.; Abdallah, J.; Khalek, S.A.; Abdelalim, A.A.; Bansil, H.S. Observation of a new particle in the search for the Standard Model Higgs boson with the ATLAS detector at the LHC. *Phys. Lett. B* **2012**, *716*, 1–29. [CrossRef]
2. Chatrchyan, S.; Khachatryan, V.; Sirunyan, A.M.; Tumasyan, A.; Adam, W.; Aguilo, E.; Da Costa, E.M. Observation of a New Boson at a Mass of 125 GeV with the CMS Experiment at the LHC. *Phys. Lett. B* **2012**, *716*, 30–61. [CrossRef]
3. CMS Collaboration. A portrait of the Higgs boson by the CMS experiment ten years after the discovery. *Nature* **2022**, *607*, 60–68 [CrossRef] [PubMed]
4. ATLAS. A detailed map of Higgs boson interactions by the ATLAS experiment ten years after the discovery. *Nature* **2022**, *607*, 52–59. [CrossRef]
5. Aad, G.; Abbott, B.; Abdallah, J.; Abeloos, B.; Aben, R.; AbouZeid, O.S.; Abraham, N.L.; Abramowicz, H.; Abreu, H.; Abreu, R.; et al. Measurements of the Higgs boson production and decay rates and constraints on its couplings from a combined ATLAS and CMS analysis of the LHC pp collision data at $\sqrt{s} = 7$ and 8 TeV. *JHEP* **2016**, *8*, 045.
6. The ATLAS Collaboration. Combined Measurements of Higgs Boson Production and Decay Using up to 80 fb^{-1} of Proton–Proton Collision Data at $\sqrt{s} = 13$ TeV Collected with the ATLAS Experiment. *Phys. Rev. D* **2020**, *101*, 012002. [CrossRef]
7. Sirunyan, A.M.; Tumasyan, A.; Adam, W.; Ambrogi, F.; Asilar, E.; Bergauer, T.; Brandstetter, J.; Dragicevic, J.; Ero, J.; Escalante Del Valle, A.; et al. [CMS], Combined measurements of Higgs boson couplings in proton–proton collisions at $\sqrt{s} = 13$ TeV. *Eur. Phys. J. C* **2019**, *79*, 421. [CrossRef]
8. Sirunyan, A.M.; Tumasyan, A.; Adam, W.; Ambrogi, F.; Asilar, E.; Bergauer, T.; Marinov, A. Observation of Higgs boson decay to bottom quarks. *Phys. Rev. Lett.* **2018**, *121*, 121801. [CrossRef]
9. Aad, G.; Abbott, B.; Abbott, D.C.; Abed Abud, A.; Abeling, K.; Abhayasinghe, D.K.; Balz, J. Search for Higgs boson production in association with a high-energy photon via vector-boson fusion with decay into bottom quark pairs at $\sqrt{s}$=13 TeV with the ATLAS detector. *JHEP* **2021**, *03*, 268. [CrossRef]
10. Clark, P.J.; Farrington, S.; Faucci Giannelli, M.; Gao, Y.; Hasib, A.; Martin, V.J.; Mijovic, L. Observation of $H \to b\bar{b}$ decays and VH production with the ATLAS detector. *Phys. Lett. B* **2018**, *786*, 59–86.
11. CMS Collaboration. Observation of the Higgs boson decay to a pair of τ leptons with the CMS detector. *Phys. Lett. B* **2018**, *779*, 283–316. [CrossRef]
12. ATLAS. Cross-Section Measurements of the Higgs Boson Decaying to a Pair of Tau Leptons in Proton–Proton Collisions at $\sqrt{s} = 13$ TeV with the ATLAS Detector. *Phys. Rev. D* **2019**, *99*, 072001. [CrossRef]
13. Bakhshiansohi, H.; Bondu, O.; Brochet, S.; Bruno, G.; Caputo, C.; David, P.; Zobec, J. Observation of $t\bar{t}$H production. *Phys. Rev. Lett.* **2018**, *120*, 231801.
14. Aaboud, M.; Aad, G.; Abbott, B.; Abeloos, B.; Abhayasinghe, D.K.; Abidi, S.H.; Barisits, M.S. Observation of Higgs boson production in association with a top quark pair at the LHC with the ATLAS detector. *Phys. Lett. B* **2018**, *784*, 173–191. [CrossRef]
15. Barbieri, R.; Giudice, G.F. Upper Bounds on Supersymmetric Particle Masses. *Nucl. Phys. B* **1988**, *306*, 63–76. [CrossRef]
16. Barbieri, R.; Hall, L.J.; Rychkov, V.S. Improved naturalness with a heavy Higgs: An Alternative road to LHC physics. *Phys. Rev. D* **2006**, *74*, 015007. [CrossRef]
17. Giudice, G.F. Naturally Speaking: The Naturalness Criterion and Physics at the LHC. *arXiv* **2008**, arXiv:0801.2562
18. Hooft, G. Naturalness, chiral symmetry, and spontaneous chiral symmetry breaking. *NATO Sci. Ser. B* **1980**, *59*, 135–157.
19. Ade, P.A.; Aghanim, N.; Arnaud, M.; Ashdown, M.; Aumont, J.; Baccigalupi, C.; Matarrese, S. Planck 2015 results. XIII. Cosmological parameters. *Astron. Astrophys.* **2016**, *594*, A13.
20. Bertone, G.; Hooper, D. History of dark matter. *Rev. Mod. Phys.* **2018**, *90*, 045002. [CrossRef]
21. Simon, J.D. The Faintest Dwarf Galaxies. *Ann. Rev. Astron. Astrophys.* **2019**, *57*, 375–415. [CrossRef]
22. Salucci, P. The distribution of dark matter in galaxies. *Astron. Astrophys. Rev.* **2019**, *27*, 2. [CrossRef]

23. Allen, S.W.; Evrard, A.E.; Mantz, A.B. Cosmological Parameters from Observations of Galaxy Clusters. *Ann. Rev. Astron. Astrophys.* **2011**, *49*, 409–470. [CrossRef]
24. Bahcall, N.A.; Cen, R.; Dave, R.; Ostriker, J.P.; Yu, Q. The Mass-to-light function: Antibias and omega(m). *Astrophys. J.* **2000**, *541*, 1. [CrossRef]
25. Mooij, S.; Shaposhnikov, M. QFT without infinities and hierarchy problem. *arXiv* **2021**, arXiv:2110.05175.
26. Bernal, N.; Heikinheimo, M.; Tenkanen, T.; Tuominen, K.; Vaskonen, V. The Dawn of FIMP Dark Matter: A Review of Models and Constraints. *Int. J. Mod. Phys. A* **2017**, *32*, 1730023. [CrossRef]
27. Bergström, L. Nonbaryonic dark matter: Observational evidence and detection methods. *Rept. Prog. Phys.* **2000**, *63*, 793. [CrossRef]
28. de Swart, J.; Bertone, G.; van Dongen, J. How Dark Matter Came to Matter. *Nat. Astron.* **2017**, *1*, 0059. [CrossRef]
29. Arcadi, G.; Dutra, M.; Ghosh, P.; Lindner, M.; Mambrini, Y.; Pierre, M.; Profumo, S.; Queiroz, F.S. The waning of the WIMP? A review of models, searches, and constraints. *Eur. Phys. J. C* **2018**, *78*, 203. [CrossRef]
30. Khlopov, M.Y. Introduction to the special issue on indirect dark matter searches. *Mod. Phys. Lett. A* **2014**, *29*, 1402001. [CrossRef]
31. Gaskins, J.M. A review of indirect searches for particle dark matter. *Contemp. Phys.* **2016**, *57*, 496–525. [CrossRef]
32. Valentino, E.D.; Melchiorri, A.; Mena, O.; Vagnozzi, S. Nonminimal dark sector physics and cosmological tensions. *Phys. Rev. D* **2020**, *101*, 063502. [CrossRef]
33. Buen-Abad, M.A.; Schmaltz, M.; Lesgourgues, J.; Brinckmann, T. Interacting Dark Sector and Precision Cosmology. *JCAP* **2018**, *2018*, 8. [CrossRef]
34. Kumar, S.; Nunes, R.C. Echo of interactions in the dark sector. *Phys. Rev. D* **2017**, *96*, 103511. [CrossRef]
35. Cirelli, M.; Panci, P.; Petraki, K.; Sala, F.; Taoso, M. Dark Matter's secret liaisons: Phenomenology of a dark U(1) sector with bound states. *JCAP* **2017**, *5*, 036. [CrossRef]
36. Berlin, A.; Hooper, D.; Krnjaic, G. PeV-Scale Dark Matter as a Thermal Relic of a Decoupled Sector. *Phys. Lett. B* **2016**, *760*, 106–111. [CrossRef]
37. Elor, G.; Rodd, N.L.; Slatyer, T.R.; Xue, W. Model-Independent Indirect Detection Constraints on Hidden Sector Dark Matter. *JCAP* **2016**, *6*, 024. [CrossRef]
38. Foot, R.; Vagnozzi, S. Dissipative hidden sector dark matter. *Phys. Rev. D* **2015**, *91*, 023512. [CrossRef]
39. Berlin, A.; Gratia, P.; Hooper, D.; McDermott, S.D. Hidden Sector Dark Matter Models for the Galactic Center Gamma-Ray Excess. *Phys. Rev. D* **2014**, *90*, 015032. [CrossRef]
40. Boddy, K.K.; Feng, J.L.; Kaplinghat, M.; Tait, T.M.P. Self-Interacting Dark Matter from a Non-Abelian Hidden Sector. *Phys. Rev. D* **2014**, *89*, 115017. [CrossRef]
41. Khlopov, M. Fundamental Particle Structure in the Cosmological Dark Matter. *Int. J. Mod. Phys. A* **2013**, *28*, 1330042. [CrossRef]
42. Cohen, T.; Phalen, D.J.; Pierce, A.; Zurek, K.M. Asymmetric Dark Matter from a GeV Hidden Sector. *Phys. Rev. D* **2010**, *82*, 056001. [CrossRef]
43. Bean, R.; Flanagan, E.E.; Laszlo, I.; Trodden, M. Constraining Interactions in Cosmology's Dark Sector. *Phys. Rev. D* **2008**, *78*, 123514. [CrossRef]
44. Ackerman, L.; Buckley, M.R.; Carroll, S.M.; Kamionkowski, M. Dark Matter and Dark Radiation. *Phys. Rev. D* **2009**, *79*, 023519. [CrossRef]
45. Arkani-Hamed, N.; Finkbeiner, D.P.; Slatyer, T.R.; Weiner, N. A Theory of Dark Matter. *Phys. Rev. D* **2009**, *79*, 015014. [CrossRef]
46. Fan, J.; Katz, A.; Randall, L.; Reece, M. Dark-Disk Universe. *Phys. Rev. Lett.* **2013**, *110*, 211302. [CrossRef]
47. Heikinheimo, M.; Raidal, M.; Spethmann, C.; Veermäe, H. Dark matter self-interactions via collisionless shocks in cluster mergers. *Phys. Lett. B* **2015**, *749*, 236–241. [CrossRef]
48. Agrawal, P.; Cyr-Racine, F.Y.; Randall, L.; Scholtz, J. Make Dark Matter Charged Again. *JCAP* **2017**, *5*, 022. [CrossRef]
49. Hewett, J.L.; Weerts, H.; Brock, R.; Butler, J.N.; Casey, B.C.K.; Collar, J.; de Gouvea, A.; Essig, R.; Grossman, Y.; Haxton, W.; et al. Fundamental Physics at the Intensity Frontier. *arXiv* **2012**, arXiv:1205.2671.
50. Essig, R.; Jaros, J.A.; Wester, W.; Adrian, P.H.; Andreas, S.; Averett, T.; Baker, O.; Batell, B.; Battaglieri, M.; Beacham, J.; et al. Working Group Report: New Light Weakly Coupled Particles. *arXiv* **2013**, arXiv:1311.0029
51. Raggi, M.; Kozhuharov, V. Results and perspectives in dark photon physics. *Riv. Nuovo Cim.* **2015**, *38*, 449–505. [CrossRef]
52. Deliyergiyev, M.A. Recent Progress in Search for Dark Sector Signatures. *Open Phys.* **2016**, *14*, 281–303. [CrossRef]
53. Alekhin, S.; Altmannshofer, W.; Asaka, T.; Batell, B.; Bezrukov, F.; Bondarenko, K.; Boyarsky, A.; Choi, K.Y.; Corral, C.; Craig, N.; et al. A facility to Search for Hidden Particles at the CERN SPS: The SHiP physics case. *Rept. Prog. Phys.* **2016**, *79*, 124201. [CrossRef] [PubMed]
54. Alexander, J.; Battaglieri, M.; Echenard, B.; Essig, R.; Graham, M.; Izaguirre, E.; Jaros, J.; Krnjaic, G.; Mardon, J.; Morrissey, D.; et al. Dark Sectors 2016 Workshop: Community Report. *arXiv* **2016**, arXiv:1608.08632
55. Beacham, J.; Burrage, C.; Curtin, D.; Roeck, A.D.; Evans, J.; Feng, J.L.; Gatto, C.; Gninenko, S.; Hartin, A.; Irastorza, I.; et al. Physics Beyond Colliders at CERN: Beyond the Standard Model Working Group Report. *J. Phys. G* **2020**, *47*, 010501. [CrossRef]
56. Albert, A.; Boveia, A.; Brandt, O.; Corrigan, E.; Demiragli, Z.; Doglioni, C.; Dreyer, E.; Gao, B.; Greaves, J.; Haisch, U.; et al. Displaying dark matter constraints from colliders with varying simplified model parameters. *arXiv* **2022**, arXiv:2203.12035.

57. Boveia, A.; Doglioni, C.; Gao, B.; Greaves, J.; Harris, P.; Pachal, K.; Dreyer, E.; Gustavino, G.; Harris, R.; Hayden, D.; et al. Summarizing experimental sensitivities of collider experiments to dark matter models and comparison to other experiments. *arXiv* **2022**, arXiv:2206.03456.
58. Rizzo, T.G. Portal Matter and Dark Sector Phenomenology at Colliders. *arXiv* **2022**, arXiv:2202.02222.
59. Alimena, J.; Beacham, J.; Borsato, M.; Cheng, Y.; Vidal, X.C.; Cottin, G.; Roeck, A.D.; Desai, N.; Curtin, D.; Evans, J.A.; et al. Searching for long-lived particles beyond the Standard Model at the Large Hadron Collider. *J. Phys. G* **2020**, *47*, 090501. [CrossRef]
60. Badertscher, A.; Crivelli, P.; Fetscher, W.; Gendotti, U.; Gninenko, S.; Postoev, V.; Rubbia, A.; Samoylenko, V.; Sillou, D. An Improved Limit on Invisible Decays of Positronium. *Phys. Rev. D* **2007**, *75*, 032004. [CrossRef]
61. Hagley, E.W.; Pipkin, F.M. Separated oscillatory field measurement of hydrogen S-21/2- P-23/2 fine structure interval. *Phys. Rev. Lett.* **1994**, *72*, 1172–1175. [CrossRef]
62. Prinz, A.A.; Baggs, R.; Ballam, J.; Ecklund, S.; Fertig, C.; Jaros, J.A.; Kase, K.; Kulikov, A.; Langeveld, W.G.J.; Leonard, R.; et al. Search for millicharged particles at SLAC. *Phys. Rev. Lett.* **1998**, *81*, 1175–1178. [CrossRef]
63. Magill, G.; Plestid, R.; Pospelov, M.; Tsai, Y.D. Millicharged particles in neutrino experiments. *Phys. Rev. Lett.* **2019**, *122*, 071801. [CrossRef]
64. Holdom, B. Two U(1)'s and Epsilon Charge Shifts. *Phys. Lett. B* **1986**, *166*, 196. [CrossRef]
65. Fayet, P. Extra U(1)'s and New Forces. *Nucl. Phys. B* **1990**, *347*, 743–768. [CrossRef]
66. Fayet, P. Effects of the Spin 1 Partner of the Goldstino (Gravitino) on Neutral Current Phenomenology. *Phys. Lett. B* **1980**, *95*, 285–289. [CrossRef]
67. Fayet, P. On the Search for a New Spin 1 Boson. *Nucl. Phys. B* **1981**, *187*, 184–204. [CrossRef]
68. Okun, L.B. Limits of electrodynamics: Paraphotons? *Sov. Phys. JETP* **1982**, *56*, 502.
69. Georgi, H.; Ginsparg, P.H.; Glashow, S.L. Photon Oscillations and the Cosmic Background Radiation. *Nature* **1983**, *306*, 765–766. [CrossRef]
70. Mougeot, X. Observation of Excess Electronic Recoil Events in XENON1T. *arXiv* **2020**, arXiv:2006.09721
71. Fuss, A.; Kaznacheeva, M.; Reindl, F.; Wagner, F.; Adari, P.; Aguilar-Arevalo, A.; Amidei, D.; Angloher, G.; Armengaud, E.; Augier, C.; et al. EXCESS workshop: Descriptions of rising low-energy spectra. *arXiv* **2022**, arXiv:2202.05097.
72. Buchalla, G.; Komatsubara, T.K.; Muheim, F.; Silvestrini, L.; Artuso, M.; Asner, D.M.; Ball, P.; Baracchini, E.; Bell, G.; Beneke, M.; et al. *B*, *D* and *K* decays. *Eur. Phys. J. C* **2008**, *57*, 309–492. [CrossRef]
73. Antonelli, M.; Asner, D.M.; Bauer, D.; Becher, T.G.; Beneke, M.; Bevan, A.J.; Blanke, M.; Bloise, C.; Bona, M.; Bondar, A.E.; et al. Flavor Physics in the Quark Sector. *Phys. Rept.* **2010**, *494*, 197–414. [CrossRef]
74. Gabrielli, E.; Raidal, M. Exponentially spread dynamical Yukawa couplings from non-perturbative chiral symmetry breaking in the dark sector. *Phys. Rev. D* **2014**, *89*, 015008. [CrossRef]
75. Gabrielli, E.; Marzola, L.; Raidal, M. Radiative Yukawa Couplings in the Simplest Left-Right Symmetric Model. *Phys. Rev. D* **2017**, *95*, 035005. [CrossRef]
76. Gabrielli, E.; Marzo, C.; Marzola, L.; Müürsepp, K. Dark origin of the quark flavor hierarchy and mixing. *Phys. Rev. D* **2020**, *101*, 075019. [CrossRef]
77. Froggatt, C.D.; Nielsen, H.B. Hierarchy of Quark Masses, Cabibbo Angles and CP Violation. *Nucl. Phys. B* **1979**, *147*, 277–298. [CrossRef]
78. Arkani-Hamed, N.; Schmaltz, M. Hierarchies without symmetries from extra dimensions. *Phys. Rev. D* **2000**, *61*, 033005. [CrossRef]
79. Gabrielli, E. On the dynamical breaking of chiral symmetry: A New mechanism. *Phys. Rev. D* **2008**, *77*, 055020. [CrossRef]
80. Gabrielli, E.; Marzola, L.; Müürsepp, K.; Ouyang, R. Vacuum stability with radiative Yukawa couplings. *JHEP* **2022**, *1*, 142. [CrossRef]
81. Bezrukov, F.; Shaposhnikov, M. Standard Model Higgs boson mass from inflation: Two loop analysis. *JHEP* **2009**, *7*, 089. [CrossRef]
82. Ellis, J.; Espinosa, J.R.; Giudice, G.F.; Hoecker, A.; Riotto, A. The Probable Fate of the Standard Model. *Phys. Lett. B* **2009**, *679*, 369–375. [CrossRef]
83. Elias-Miro, J.; Espinosa, J.R.; Giudice, G.F.; Isidori, G.; Riotto, A.; Strumia, A. Higgs mass implications on the stability of the electroweak vacuum. *Phys. Lett. B* **2012**, *709*, 222. [CrossRef]
84. Isidori, G.; Rychkov, V.S.; Strumia, A.; Tetradis, N. Gravitational corrections to standard model vacuum decay. *Phys. Rev. D* **2008**, *77*, 025034. [CrossRef]
85. Mihaila, L.N.; Salomon, J.; Steinhauser, M. Gauge Coupling Beta Functions in the Standard Model to Three Loops. *Phys. Rev. Lett.* **2012**, *108*, 151602. [CrossRef] [PubMed]
86. Degrassi, G.; Vita, S.D.; Elias-Miro, J.; Espinosa, J.R.; Giudice, G.F.; Isidori, G.; Strumia, A. Higgs mass and vacuum stability in the Standard Model at NNLO. *JHEP* **2012**, *8*, 098. [CrossRef]
87. Chetyrkin, K.G.; Zoller, M.F. Three-loop beta-functions for top-Yukawa and the Higgs self-interaction in the Standard Model. *JHEP* **2012**, *6*, 033. [CrossRef]
88. Fabbrichesi, M.; Gabrielli, E.; Lanfranchi, G. *The Physics of the Dark Photon. A Primer*; SpringerBriefs in Physics; Springer: Berlin/Heidelberg, Germany, 2020.
89. Lagouri, T. Review on Higgs hidden-dark sector physics. *Phys. Scripta* **2022**, *97*, 024001. [CrossRef]
90. Dobrescu, B.A. Massless gauge bosons other than the photon. *Phys. Rev. Lett.* **2005**, *94*, 151802. [CrossRef]

91. Gabrielli, E.; Heikinheimo, M.; Mele, B.; Raidal, M. Dark photons and resonant monophoton signatures in Higgs boson decays at the LHC. *Phys. Rev. D* **2014**, *90*, 055032. [CrossRef]
92. Biswas, S.; Gabrielli, E.; Heikinheimo, M.; Mele, B. dark photon searches via Higgs boson production at the LHC. *Phys. Rev. D* **2016**, *93*, 093011. [CrossRef]
93. Aad, G.; Abbott, B.; Abbott, D.C.; Abud, A.A.; Abeling, K.; Abhayasinghe, D.K.; Balek, P. Observation of electroweak production of two jets in association with an isolated photon and missing transverse momentum, and search for a Higgs boson decaying into invisible particles at 13 TeV with the ATLAS detector. *Eur. Phys. J. C* **2022**, *82*, 105.
94. Sirunyan, A.M.; Tumasyan, A.; Adam, W.; Bergauer, T.; Dragicevic, M.; Erö, J.; Yuan, L. Search for dark photons in Higgs boson production via vector boson fusion in proton-proton collisions at $\sqrt{s}$ = 13 TeV. *JHEP* **2021**, *3*, 011. [CrossRef]
95. Sirunyan, A.M.; Tumasyan, A.; Adam, W.; Ambrogi, F.; Bergauer, T.; Br Stetter, J.; Chen, G.M. Search for dark photons in decays of Higgs bosons produced in association with Z bosons in proton-proton collisions at $\sqrt{s}$ = 13 TeV. *JHEP* **2019**, *10*, 139.
96. Biswas, S.; Gabrielli, E.; Heikinheimo, M.; Mele, B. Higgs boson production in association with a dark photon in e^+e^- collisions. *JHEP* **2015**, *6*, 102. [CrossRef]
97. Biswas, S.; Gabrielli, E.; Heikinheimo, M.; Mele, B. dark photon searches via ZH production at e^+e^- colliders. *Phys. Rev. D* **2017**, *96*, 055012. [CrossRef]
98. D'Ambrosio, G.; Giudice, G.F.; Isidori, G.; Strumia, A. Minimal flavor violation: An Effective field theory approach. *Nucl. Phys. B* **2002**, *645*, 155–187. [CrossRef]
99. CMS Collaboration. Search for invisible decays of the Higgs boson produced via vector boson fusion in proton-proton collisions at $\sqrt{s} = 13$ TeV. *Phys. Rev. D* **2022**, *105*, 092007. [CrossRef]
100. ATLAS Collaboration. Search for invisible Higgs boson decays in events with vector-boson fusion signatures using 139 fb^{-1} of proton-proton data recorded by the ATLAS experiment. *arXiv* **2022**, arXiv:2202.07953.
101. Yao, W.M.; Amsler, C.; Asner, D.; Barnett, R.M.; Beringer, J.; Burchat, P.R.; Staney, T. Review of Particle Physics. *PTEP* **2020**, *2020*, 083C01.
102. Fierz, M.; Pauli, W. On relativistic wave equations for particles of arbitrary spin in an electromagnetic field. *Proc. Roy. Soc. Lond. A* **1939**, *A173*, 211–232.
103. Han, T.; Lykken, J.D.; Zhang, R.J. On Kaluza-Klein states from large extra dimensions. *Phys. Rev. D* **1999**, *59*, 105006. [CrossRef]
104. Giudice, G.F.; Rattazzi, R.; Wells, J.D. Quantum gravity and extra dimensions at high-energy colliders. *Nucl. Phys. B* **1999**, *544*, 3–38. [CrossRef]
105. Comelato, A.; Gabrielli, E. Untangling the spin of a dark boson in Z decays. *Phys. Rev. D* **2020**, *102*, 015028. [CrossRef]
106. Result provided by D. Anselmi in private communications. For $D = 4$ see C. Fronsdal, Massless Fields with Integer Spin. *Phys. Rev. D* **1978**, *18*, 3624.
107. Beauchesne, H.; Chiang, C.W. Measuring properties of a dark photon from semi-invisible decay of the Higgs boson. *JHEP* **2022**, *4*, 127. [CrossRef]
108. Heinemeyer, S.; Mariotti, C.; Passarino, G.; Tanaka, R.; Andersen, J.R.; Artoisenet, P.; Yu, J. Handbook of LHC Higgs Cross Sections: 3. Higgs Properties. CERN Yellow Reports: Monographs. *arXiv* **2013**, arXiv:1307.1347.
109. Mangano, M.L.; Moretti, M.; Piccinini, F.; Pittau, R.; Polosa, A.D. ALPGEN, a generator for hard multiparton processes in hadronic collisions. *JHEP* **2003**, *7*, 001. [CrossRef]
110. Alwall, J.; Frederix, R.; Frixione, S.; Hirschi, V.; Maltoni, F.; Mattelaer, O.; Shao, H.S.; Stelzer, T.; Torrielli, P.; Zaro, M. The automated computation of tree-level and next-to-leading order differential cross sections, and their matching to parton shower simulations. *JHEP* **2014**, *7*, 079. [CrossRef]
111. Sjostrand, T.; Mrenna, S.; Skands, P.Z. PYTHIA 6.4 Physics and Manual. *JHEP* **2006**, *5*, 026. [CrossRef]
112. Biswas, S.; Gabrielli, E.; Heikinheimo, M.; Mele, B. Searching for massless Dark Photons at the LHC via Higgs boson production. *PoS* **2017**, *EPS-HEP2017*, 315.
113. Vidal, X.C.; D'Onofrio, M.; Fox, P.J.; Torre, R.; Ulmer, K.A.; Aboubrahim, A.; Albert, A.; Alimena, J.; Allanach, B.C.; Alpigiani, C.; et al. Report from Working Group 3: Beyond the Standard Model physics at the HL–LHC and HE–LHC. *CERN Yellow Rep. Monogr.* **2019**, *7*, 585–865.
114. FCC Collaboration. FCC-ee: The Lepton Collider: Future Circular Collider Conceptual Design Report Volume 2. *Eur. Phys. J. ST* **2019**, *228*, 261–623. [CrossRef]
115. Alloul, A.; Christensen, N.D.; Degrande, C.; Duhr, C.; Fuks, B. FeynRules 2.0—A complete toolbox for tree-level phenomenology. *Comput. Phys. Commun.* **2014**, *185*, 2250–2300. [CrossRef]